8-2013

Synthesis of Platinum and Platinum-Copper Branched Nanoparticles for Electrooxidation of Methanol

Eric Courtland Taylor
University of Arkansas, Fayetteville

SYNTHESIS OF PLATINUM AND PLATINUM-COPPER BRANCHED NANOPARTICLES FOR ELECTROOXIDATION OF METHANOL

SYNTHESIS OF PLATINUM AND PLATINUM-COPPER BRANCHED NANOPARTICLES FOR ELECTROOXIDATION OF METHANOL

A thesis submitted in partial fulfillment
of the requirements for the degree of
Master of Science in Chemistry

By

Eric Taylor
University of the Cumberlands
Bachelor of Science in Chemistry, 2010

August 2013
University of Arkansas

This thesis is approved for recommendation to the Graduate Council

_____
Dr. Jingyi Chen
Thesis Director

_____
Dr. Colin Heyes
Committee Member

_____
Dr. Ingrid Fritsch
Committee Member

ABSTRACT

Platinum and Pt alloys are among the most important heterogeneous catalysts for many organic reactions and electrochemical reactions associated with the fuel cell technologies. How to reduce Pt usage while maintaining the performance of the catalysts becomes a subject for intensive research in materials chemistry. For heterogeneous catalysis, the catalytic reactivity and selectivity are strongly correlated with different crystallographic facets exposed on the surface. The facets with high-index planes whose Miller indices with at one is larger than unity are generally more active than those with low-index planes (e.g., {100}, {111}, and {110}). Tuning the morphology of the nanoparticles to expose more high-index planes on the surface can improve the catalytic activity of the nanoparticles. As compared to isotropic nanoparticles, the branched nanostructures are the promising morphology that can improve both the activity and stability of the catalysts. In this work, a two-step polyol synthesis has been developed to synthesize the branched nanostructures of Pt at high-yield. This two-step process involves a slow reduction using ethylene glycol in the presence of oxidative etchants, following by a fast reduction using ascorbic acid. The slow reduction kinetics facilitates the formation of cubooctahedral single-crystal seeds while the fast reduction kinetics allows for the overgrowth of nanocrystals along the {111} facets in a short period of time, resulting in the branched nanostructures. By co-reducing Pt and Cu precursors, this approach has been demonstrated to synthesize the Pt-Cu dendritic nanostructures for the first time. The catalytic activity of these Pt and Pt-Cu nanostructures has been studied for MOR. It was found that Pt branched nanostructures reduced the CO-poisoning as compared to the Pt/C and the dendritic Pt-Cu nanostructures showed both enhanced resistance of CO-poisoning and improved efficiency of ethanol oxidation.

ACKNOWLEDGMENTS

Firstly I would like to thank parents and sister for all of their encouragement during my time in college and graduate school. There was many a time that I did not think that I could pull through the struggles I was experiencing but my mother was always there to give me a pep talk. My father was a great well of knowledge and understanding while working on this thesis giving me the faith that I could power through any of the obstacles that lay in my way.

Academically, I'd like to than my Master's Advisor, Dr. Jingyi Chen, she has taught me a great deal about having a good work ethic and that through hard work produces great reward. She has helped me so much in my studies in physical chemistry and understanding how to tackle any research problems that occurred. Special thanks to Dr. Ingrid Fritsch, you class on electrochemistry has been so useful to my research and has open my eyes to the power of this field in the investigation of nanomaterials as well as the support you have given me while writing me thesis. I would also like to thank Dr. Colin Heyes for his course on single molecular spectroscopy. The knowledge that I learned in that course has helped in understand the power of many tools that I had previously not been exposed to for use in nanomaterials and also his general friendly nature whenever we were to have a conversation or just pass in the hall.

To the present Chen group members, I enjoyed working with you all for these last several years. Dr. Shutang Chen, you are a great friend and colleague. It seems that everything you do is selfless and that is something to strive toward. All of your knowledge and fun personality helped me get through some of the worst days and I hope that you, your wife, and your daughter have a wonderful life. I hope that all of your research has much progress and wish you the best of luck in your carriers during and after working in our research group.

DEDICATION

To my grandfather who always believed in me. He always taught me to do your best that's all you can ever be expected to do. I wish that he was here to see his grandson be able to succeed so much in life.

TABLE OF CONTENTS

LIST OF ABBREVIATIONS

PVP 55K	Polyvinylprrolidone MW~55K
PVP 40K	Polyvinylprrolidone MW~40K
PVP 8K	Polyvinylprrolidone MW~8K
EG	Ethylene Glycol
PEG	Polyethylene Glycol
AA	Ascorbic Acid
HAc	Acetic Acid
Ag/AgCl	Silver / Silver Chloride
GA	Glycolaldehyde
EtOH	Ethanol
MeOH	Methanol
MOR	Methanol Oxidation Reaction
ORR	Oxygen Reduction Reaction
TEM	Transmission Electron Microscopy
Rcf	Relative Centrifugal Force
UV-vis	Ultra Violate-visible
CV	Cyclic Voltammetry
CA	Chronoamperometry
ECSA	Electrochemical Surface Area
DEG	Diethylene Glycol
PEMFC	Proton Exchange Membrane Fuel Cell
AAS	Atomic Absorption Spectroscopy
Pt-B	Platinum Branched Nanostructures
Pt/C	Carbon supported platinum nanoparticles

Chapter 1: Introduction

1.1. The Importance of Platinum and Their Alloys

Platinum is a precious transition metal that has excellent catalytic and electrical properties, as well as superior resistant characteristics to corrosion. It has been widely used as catalysts in chemical,[1] petrochemical,[2] pharmaceutical,[3] electronic,[4] and automotive industries.[5] For example, Pt can effectively catalyze many organic reactions such as in isomerization[6] and hydrogenation.[3] Platinum is one of the three main components the catalytic converter in exhaust system for automobile to oxidize the toxic pollutants (e.g. CO) to less toxic compounds (e.g. CO_2). Platinum is the best monometallic catalysts for fuel cell applications. It is often used as the gold standard for the comparison of catalytic activities for the half-reactions related to the fuel cell technologies, such as oxygen reduction reaction (ORR), hydrogen oxidation reaction, methanol oxidation reaction (MOR), formic acid oxidation reaction (FAOR), and ethanol oxidation reaction (EOR).[7, 8, 9] Being a precious metal, Pt is costly which leads to the high cost of the Pt-based technologies.[10] For commercialization, it is important to reduce the cost of catalysts by increasing the mass activity of Pt or completely eliminate the use of non-precious metal. The performance of the catalysts without non-precious metals is very poor compared to Pt. Therefore, the scope of this work focuses on the improvement of catalytic performance of Pt catalysts. The mass activity of Pt can be improved by increasing the number of active sites in pure Pt nanocrystals and/or by alloying Pt with the low-cost metal (i.e. Cu). The goal is to synthesize Pt and Pt-Cu nanostructures with enhanced catalytic properties. The catalytic performance of the nanostructures is evaluated on MOR, the anode reaction in the direct methanol fuel cell (DMFC).

1.2. Synthesis of Platinum and Their Alloys

1.2.1. Synthesis Platinum Nanostructures

For pure Pt catalyst, the catalytic property can be tuned by the morphology of nanoparticles.

The facets with large amount of steps, ledges, and kinks are catalytically more active than the low index facets, such as {100}, {111}, and {110}.[11] The atoms at steps, ledges and kinks have less neighbor atoms or low coordination number.[12] This alters their electronic structures, resulting in the change of catalytic reactivity and selectivity. In the past two decades, much progress has been made on the synthesis of Pt nanostructures. El-Sayed and co-workers were the first to demonstrate the shape-controlled synthesis of Pt nanoparticles.[1] In this method, the final shape of Pt was controlled by changing the concentration of the capping ligand and the pH of the reaction solution. By tuning these parameters, several shapes of Pt were obtained including tetrahedra, polyhedra, and cubes. Many efforts have been devoted to the shape-controlled synthesis of Pt nanoparticles based off of the result found in those early experiments. The Pt nanostructures are synthesized by reducing a Pt precursor in different solvent systems such as aqueous solution, polyol, or non-polar solvents.

Figure 1-1 summarizes various shapes of single crystalline Pt that have already been made and their relationship. Pt possesses a face-centered-cubic (fcc) crystal structure. For such structure, the surface energies associated with the low-index crystallographic planes are in the order of $\gamma(111) < \gamma(100) < \gamma(110)$.[13] Based on Wulff construction mechanism, the thermodynamically-favored shape is the truncated octahedron.[14] The optimal truncation meets the condition of $\gamma(100)/\gamma(111) = d(100)/d(111)$, where d represents the distance from the facet to the center of the particle and this parameter reflects the ratio of growth rates along {100} and {111} directions.[15] The ratio of these two growth rates can be defined as R, which changes from 0.58 for a cube to 0.87 for a cuboctahedron and 1.73 for an octahedron. It is possible to alter surface energies by changing the capping ligand and/or oxidative etching, thereby changing the growth rates along different directions. As a result, different morphologies were obtained, such as cubes bounded by {100}, as well as octahedra and tetrahedra bounded by {111}.[15] The

polyhedra can evolve into multipods through overgrowth from the corners of polyhedra by controlling the reduction kinetics. On the other hand, if the initial seeds adopt a twinned structure rather than single-crystalline structure, the resultant final shapes of the nanocrystals are found to be decahedra and icosahedra.[16] However, the twinned structures have high internal energies and surface defects. As a result, they are easily to be oxidized in the case of Pt.[17]

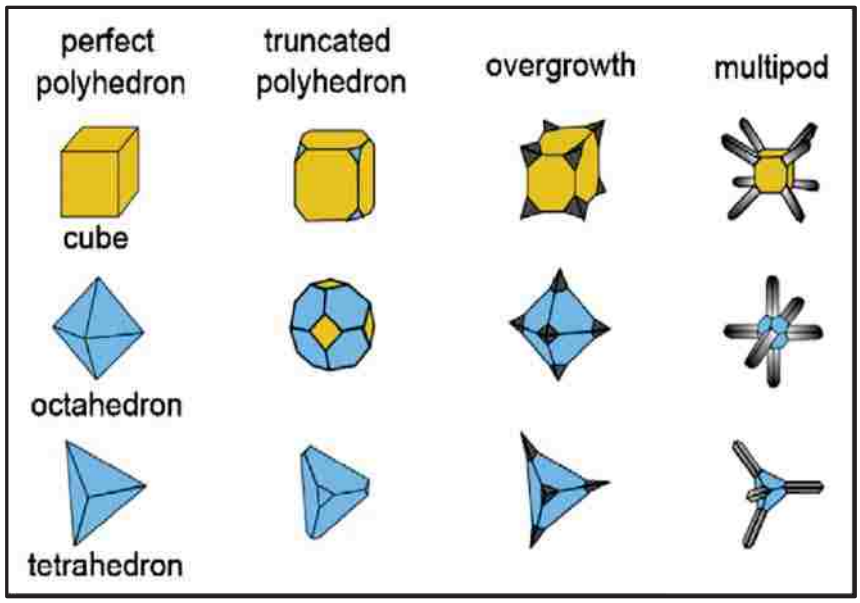

Figure 1-1. Commonly observed Pt single crystal nanostructures.

The presence of oxidative etchants is essential to control the overgrowth of Pt on the single-crystalline seeds. In this case, the twinned seeds could be eliminated from the initial nucleation step by the oxidizing agents. The reduction kinetics becomes very slow because the single crystal nuclei can be oxidized by the etchant back into Pt ions. In order for overgrowth to occur, two criteria have to be met: a low concentration of seeds and a high concentration of free Pt ions. As a result, the Pt precursors then slowly reduced and deposited onto the more energetically favorable {111} facets and grow along the <111> to become branched overgrowth nanostructures.[18] If one or more {111} directions were blocked due to the coalescence of particles, it is possible to stimulate the growth in one dimension and result in the formation of nanowires.[19] The one-dimensional structures are expected to enhance the catalytic activity and stability as compared to nanoparticles.[20] Recently, Wang and co-workers have demonstrated for the first time that the tetrahexahedra enclosed by

high-index facets (e.g., {730}, {210}, and {520}) were synthesized by electrochemical treatment of Pt nanospheres.[12] Although it is hard to scale up this approach the production of Pt nanostructures, the existence of these high-index facets provide more active sites for improving the electrocatalytic activity as compared to the nanoparticles.

1.2.2. Synthesis of Pt Alloys

Co-reduction method is general used for the synthesis of Pt alloyed nanoparticles, such as, Pt-Co[21], Pt-Ni[22], Pt-Cu[23], Pt-Pd[24] and Pt-Fe[25]. The structures of bimetallic NCs are complicated and multiform. According to the mixing pattern of two different metals, three main types of structures can be identified for bimetallic NCs, that is, core/shell, heterostructure, or intermetallic and alloyed structures.[26] For the formation of core/shell one type of metal ion is reduced first and forms the inner core, another type of metal atoms prefers to nucleate and grow surrounding the core to form a shell because separate nucleation is more difficult. Under certain conditions they grow of two types of metal atoms can occur. If the two metals share a mixed interface during the growth process heterostructure form. For intermetallics and alloys are different from these other two nanocrystals. Intermetallics and alloys are a homogeneous mixture of two metals and metal-metal bonds form.[27] In a co-reduction method for forming intermetallic or alloyed nanocrystals generally the process of reducing two metal salts together in a solvent is used. However, it is difficult to simultaneously control the reduction and nucleation process of two types of metals because their redox potential and chemical behaviors are different. In order to avoid separate nucleation of two metals, a proper reducing agent and reaction system must be selected.[28] If a strong reducing agent such as hydrazine is used both metals can be reduced at the same time. However, if there is an absence of a proper surfactant it becomes difficult to separate the nucleation and growth process as well as prevent the particles from aggregating. In some experiments it has been found that using a very strong reducing agent like $NaBH_4$ can cause

many aggregates. These aggregates are caused by the fact that the two types of metal ions are reduced instantly in the reaction solution which results in separated nucleation of the metals.[29] Using $NaBH_4$ can still be used for the co-reduction method to form alloys when the correct surfactants or polymeric ligands are selected. Schaak and co-workers have done a series of excellent work on controllable synthesis of nanocrystalline bimetallic compounds by co-reduction method using $NaBH_4$ as the reducing agent.[30]

Usually a weak reducing agent is used as it is more controllable during the co-reduction process. Yang and co-workers have synthesized Pt_3Ni nanocrystals with exposed {111} facets using $Pt(acac)_2$ and $Ni(acac)_2$ as the precursors and borane-tert-butylamine complex (TBAB) and hexadecanediol as the reducing agents.[31] The main strategy for controlling the structure of bimetallic nanocrystals using co-reduction is utilizing the different redox potentials of the two metals. Generally, the metal species with higher redox potential are reduced first. After the reduction of the second metal, its chemical behavior determines the final structure of products. When the second metal atoms diffuse into the crystal lattice of the first metal and lead to the formation of metal-metal bonds, intermetallic or alloyed compounds will be synthesized.[26] The co-reduction process in solution system is very effective in preparing high-quality NCs with tunable size because the growth rate of clusters can be well controlled by adding proper surfactants, polymers, foreign ions, or ligands and adjusting other reaction parameters which can affect the redox potentials of the metals in the solution. Recently the Schaak group has been able to synthesize Cu-Pt nanorods with tunable size. The reaction consist of the metal salt precursors in a solution of oleic acid, oleylamine, and octadecene.[32] The oleylamine is important as it can stabilize the {100} facets and leads to crystal growth along the {111} direction. As a result the concentration of the oleylamine can influence the size of the nanorods. The influence is presumably due to the different adsorption energy to the crystal surface among these surfactants

and solvents which can inhibit the incorporation rate of growth units onto the crystal surfaces and change relative crystal growth rates.[26] Using a similar synthesis Xia has found that the morphology of the nanocrystals can be controlled using the co-reduction method.[33] Their group found that the control over crystal structure and final shape of Pd-Pt bimetallic NCs could be achieved via a kinetically controlled co-reduction synthesis using different reducing agents such as PVP and ethylene glycol (EG). PVP is a weak reducing reagent and slow the nucleation of the atoms making the formed clusters in the nucleation stage more easily coalesce which can create twinned nuclei. The subsequent growth of twinned nuclei will lead to the formation of star-shaped decahedrons and triangular nanoplates with truncation at twin boundaries.[34] In comparison, when EG is used as the reducing agent instead of PVP, a co-reduction process at a relatively high rate will occur. The fast formation of metal atoms leads to a drastic increase of the degree of initial supersaturation and therefore the rapid growth of the nuclei. They finally evolve into single crystal with a truncated octahedral shape enclosed by a mix of {111} and {100} planes.[16]

The composition of bimetallic NCs can be usually controlled by changing the molar ratio of two metal precursors. However, the composition of final products is not exactly consistent with the feeding ratio in most cases due to the incomplete diffusion of the second metal into the first preformed metal. The diffusion process is greatly influenced by the reaction temperature, time, and some other factors.[26] A recent example by the Sun group synthesized Au-Ag alloy nanoparticles in which the molar ration of the $AgNO_3$ and $HAuCl_4$ were used at 10:1 molar ratio.[35] The metals were reduced using an oleylamine and octadecene method like the one described by the Schaak group. The resulting alloy was $Au_{0.82}Ag_{0.18}$ because the redox potential of Au is much higher than Ag only a small portion of Ag was incorporated into the alloy. When they prolonged the reaction time from 0.5 h to 1 h the alloy formed had more Ag than before,

$Au_{0.60}Ag_{0.40}$. They also saw that by changing the precursor $AgNO_3$ and $HAuCl_4$ ratios from 10:1 mol ratio to 20:1 mol ratio the resulting ratio was $Au_{0.39}Ag_{0.61}$.

Other groups have found that changing the mol ratio of the metal precursor can also have an influence on the final shape of the nanocrystals this is due to there being a difference in thermodynamic and kinetic characteristics between two metals in alloys.[26] The Yang group has found that the formation of Pt-Ag nanowires by co-reduction of $Pt(acac)_2$ and silver stearate (Ag(St)) using oleic acid and oleylamine can have very different final crystalline shapes and compositions depending on if the precursor mol ratio is increased or decreased.[36] According to their transmission electron microscope (TEM) results, the growth of nanowires undergoes an oriented attachment process which is mostly driven by the interplay between the binding energy of capping agents on alloy surfaces and the diffusion of atoms at the interface upon the collision of primary nanoparticles. Other factors in the reaction were also contributing but no conclusion to what exactly was the cause was determined but the mol ratio of the precursor had a large impact on the final shape.[36] These co-reduction synthesis methods are complex and have many factors impacting the results. Each system takes great time and effort to investigate the entire mechanism of growth and alloy formation.

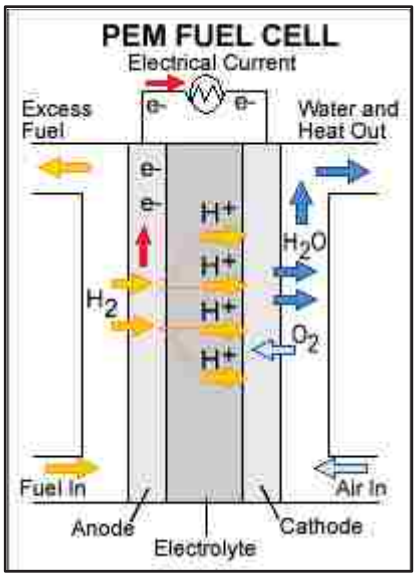

Figure 1-2. Simplified general photovoltaic cell construction.[5]

1.3. Platinum and Their Alloys for Fuel Cell Applications

1.3.1. Fuel Cells

The fuel cell is an emerging technology for energy conversion using the renewable energy sources. There are different types of fuel cell, such as alkali (AFC), molten carbonate (MCFC),

phosphoric acid (PAFC), solid oxide (SOFC), and proton exchange membrane (PEMFC). Among them, PEMFC is the most promising technology for commercialization as power supply source for automobiles and portable electronic devices. The PEMFC consist of two electrode compartments: anode and cathode with a PEM for separation that allows proton transferring from anode to cathode (Fig. 1-2). In this case, hydrogen is used as fuel. The two half reactions for hydrogen PEMFC are as follows:

Anode: $H_2 \rightarrow 2H^+ + 2e^-$ (1)

Cathode: $½O_2 + 2H^+ + 2e^- \rightarrow H_2O$ (2)

Overall: $H_2 + ½O_2 \rightarrow H_2O$ (3)

During operation, water vapor is the only product of the hydrogen PEMFC. Therefore, this technology is a truly "clean technology." However, the production, transportation, and storage of H_2 remain to be challenging in its practical use.[37]

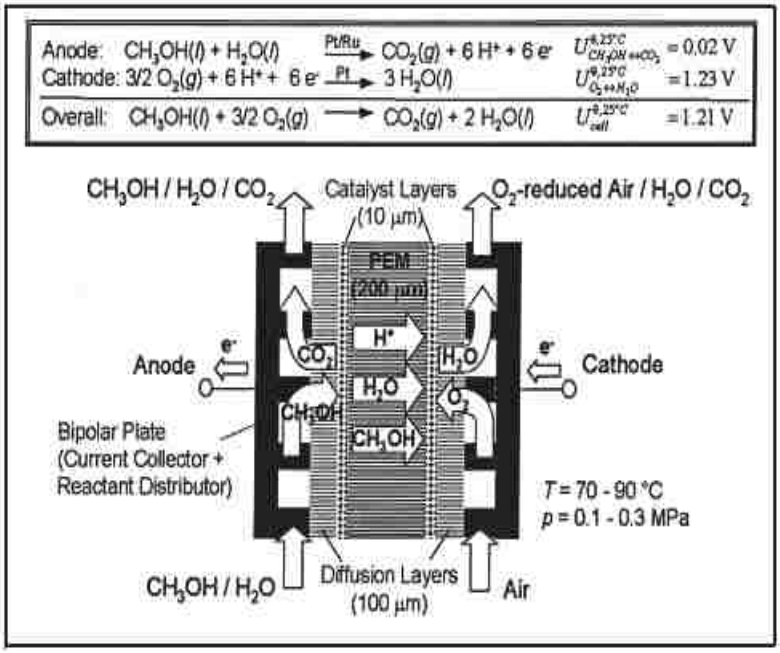

Figure 1-3. Reaction scheme and schematic of direct methanol fuel cell.[10]

Alternatively, the H_2 fuel can be replaced by small organic molecules, such as methanol, to assemble as direct methanol fuel cell (DMFC), as shown in Figure 1-3. This type of fuel cell has drawn much attention over the last twenty years due to their ability to use a more stable fuel source while still maintaining reasonable power output.[38] In this case, the anode reaction in acidic medium is as follows:

Anode: $CH_3OH + H_2O \rightarrow CO_2 + 6H^+ + 6e^-$ (4)

Theoretically, the reduction potential of methanol is the same order of that of hydrogen, making methanol a good candidate to generate the similar cell potential output.[39] However, the oxidation of methanol on the Pt has very slow kinetics, although Pt is by far the most active monometallic catalyst for this reaction. The slow kinetics requires high overpotential for the methanol oxidation to occur, thereby reducing the overall cell output potential. It has been found that the slow kinetics was the result of incomplete oxidation, yielding the intermediates. These intermediates poison the Pt catalysts and largely reduce the catalytic activity. Therefore, we use the electrooxidation of methanol as a model reaction to test the performance of our catalysts.

1.3.2. Electrooxidation of Methanol

There are different pathways involving several intermediates in the electrooxidation of methanol. The mechanism is proposed as follows.[38, 40]

$$Pt + (CH_3OH) \rightarrow Pt\text{-}(CH_3OH)_{ad} \quad (5)$$

$$Pt\text{-}(CH_3OH)_{ad} \rightarrow Pt\text{-}(\bullet CH_2OH)_{ad} + H^+_{aq} + e^- \quad (6a)$$

or

$$Pt\text{-}(CH_3OH)_{ad} \rightarrow Pt\text{-}(CH_3O\bullet)_{ad} + H^+_{aq} + e^- \quad (6b)$$

$$Pt\text{-}(\bullet CH_2OH)_{ad} \rightarrow Pt\text{-}(\bullet CHOH)_{ad} + H^+_{aq} + e^- \quad (7a)$$

or

$$Pt\text{-}(CH3O\bullet)_{ad} \rightarrow Pt\text{-}(CH_2O\bullet)_{ad} + H^+_{aq} + e^- \quad (7b)$$

$$Pt\text{-}(\bullet CHOH)_{ad} \rightarrow Pt\text{-}(\bullet CHO)ads + H^+_{aq} + e^- \quad (8a)$$

or

$$Pt\text{-}(CH_2O\bullet)_{ad} \rightarrow Pt\text{-}(\bullet CHO)_{ad} + H^+_{aq} + e^- \quad (8b)$$

The $(\bullet CHO)_{ad}$ could be dissociated on pure platinum according to the following reaction:

$$Pt\text{-}(\bullet CHO)_{ad} \rightarrow Pt\text{-}(\bullet CO)_{ad} + H^+_{aq} + e^- \quad (9)$$

The strongly adsorbed CO-like species formed during reaction 9 are the major poisoning species.[40] In order to weaken the adsorption of CO-like species on Pt electrode, an oxophilic metal (e.g. Ru) was proposed to alloy with Pt to activate H_2O for methanol oxidation described as a bifunctional mechanism.

$$Ru + H_2O \rightarrow OH_{ad} + H^+ + e^- \quad (10)$$

and

$$CO_{ad} + OH_{ad} \rightarrow CO_2 + H^+ + e^- \quad (11)$$

The presence of Ru in the alloy allows for the activation of water in the reaction mixture, to form adsorbed hydroxyl species on the catalyst surface. The adsorbed hydroxyl species on Ru react with the adsorbed CO species on Pt, forming CO_2, easily desorbed from the surface of the catalysts as in reaction 11. Although Pt-Ru catalysts largely resist the CO-poisoning, the overpotential remains high and the catalysts are still costly due to the use of precious metals. There is still room to improve the mass activity of catalysts with reduced cost for methanol oxidation.

1.4. Objectives and Overviews

The objective of this work is to develop synthetic methodology for preparation of Pt and Pt-alloys with branched nanostructures as promising catalysts for heterogeneous catalysis. In this work, a two-step polyol synthesis has been developed to synthesize the branched nanostructures of Pt at high-yield. The reaction mechanism is systematically studied to optimize the reaction parameter for the production of branched nanostructures. This newly-developed protocol is further developed for co-reduction of Pt and other metal precursors to synthesize the alloyed dendritic nanostructures with initial demonstration of Pt-Cu. The catalytic performance of these nanostructures is investigated using methanol electrooxidation and the structure-property relationship is established.

1.5. References

1. Ahmadi, T. S., Wang, Z. L., Green, T. C., Henglein, A., El-Sayed, M. A., Shape-Controlled Synthesis of Colloidal Platinum Nanoparticles. *Science* **1996,** *272*, 1924-1925.

2. J. Lipkowski, P.N. Ross, Electrocatalysis, Wiley-VCH, New York, **1998**.

3. Jones, W. H., Platinum and Palladium in the Pharmaceutical Industry. *Platinum Met. Rev.* **1958,** *2*.

4. Lu, W., Mi, B. X., Chan, M. C. W., Hui, Z., Che, C. M., Zhu, N., Lee, S. T., Light-Emitting Tridentate Cyclometalated Platinum(II) Complexes Containing σ-Alkynyl Auxiliaries: Tuning of Photo- and Electrophosphorescence. *J. Am. Chem. Soc.* **2004,** *126*, 4958-4971.

5. Gasteiger, H. A., Kocha, S. S., Sompalli, B., Wagner, F. T., Activity benchmarks and requirements for Pt, Pt-alloy, and non-Pt oxygen reduction catalysts for PEMFCs. *App. Catal., B* **2005,** *56*, 9-35.

6. Iglesia, E., Soled, S. L., Kramer, G. M., Isomerization of Alkanes on Sulfated Zirconia: Promotion by Pt and by Adamantyl Hydride Transfer Species. *J. Catal.* **1993,** *144*, 238-253.

7. (a) Stamenkovic, V. R., Fowler, B., Mun, B. S., Wang, G., Ross, P. N., Lucas, C. A., Marković, N. M., Improved Oxygen Reduction Activity on $Pt_3Ni(111)$ via Increased Surface Site Availability. *Science* **2007,** *315*, 493-497; (b) Formo, E., Peng, Z., Lee, E., Lu, X., Yang, H., Xia, Y., Direct Oxidation of Methanol on Pt Nanostructures Supported on Electrospun Nanofibers of Anatase. *J. Phys. Chem. C.* **2008,** *112*, 9970-9975.

8. Gasteiger, H. A., Markovic, N., Ross, P. N., Cairns, E. J., Methanol electrooxidation on well-characterized platinum-ruthenium bulk alloys. *J. Phys. Chem. A.* **1993,** *97*, 12020-12029.

9. Ammam, M., Easton, E. B., Quaternary PtMnCuX/C (X = Fe, Co, Ni, and Sn) and PtMnMoX/C (X = Fe, Co, Ni, Cu and Sn) alloys catalysts: Synthesis, characterization and activity towards ethanol electrooxidation. *J. Power Sources* **2012,** *215*, 188-198.

10. NASDAQ Nasdaq Stock Market, **2013**. http://www.nasdaq.com/markets/platinum.aspx.

11. Taylor, B., *J. Amer. Chem. Soc.* **1924,** *46*, 43.

12. Tian, N., Zhou, Z. Y., Sun, S. G., Ding, Y., Wang, Z. L., Synthesis of Tetrahexahedral Platinum Nanocrystals with High-Index Facets and High Electro-Oxidation Activity. *Science* **2007,** *316*, 732-735.

13. Wang, Z. L., Transmission Electron Microscopy of Shape-Controlled Nanocrystals and Their Assemblies. *J. Phys. Chem., B* **2000,** *104*, 1153-1175.

14. R. F. Strickland, Constable: Kinetics and Mechanism of Crystallization, page 77, Academic Press, **1968**.

15. Chen, J., Lim, B., Lee, E. P., Xia, Y., Shape-controlled synthesis of platinum nanocrystals for catalytic and electrocatalytic applications. *Nano Today* **2009,** *4*, 81-95.

16. Xia, Y., Xiong, Y., Lim, B., Skrabalak, S. E., Shape-Controlled Synthesis of Metal Nanocrystals: Simple Chemistry Meets Complex Physics? *Angew. Chem. Int. Ed.* **2009,** *48*, 60-103.

17. Xiong, Y., Chen, J., Wiley, B., Xia, Y., Aloni, S., Yin, Y., Understanding the Role of Oxidative Etching in the Polyol Synthesis of Pd Nanoparticles with Uniform Shape and Size. *J. Am. Chem. Soc.* **2005,** *127*, 7332-7333.

18. Chen, J., Herricks, T., Xia, Y., Polyol Synthesis of Platinum Nanostructures: Control of Morphology through the Manipulation of Reduction Kinetics. *Angew. Chem. Int. Ed.* **2005,** *44*, 2589-2592.

19. Chen, J., Herricks, T., Xia, Y., Single-Crystal Nanowires of Platinum Can Be Synthesized by Controlling the Reaction Rate of a Polyol Process. *J. Am. Chem. Soc.* **2004,** *126*, 10854-10855.

20. Chen, Z., Yan, Y., Supportless Pt and PtPd Nanotubes as Electrocatalysts for Oxygen-Reduction Reactions. *Angew. Chem.* **2007,** *119*, 4138.

21. A. Kumbhar, L. Spinu, F. Agnoli, K.Y. Wang, W.L. Zhou, C.J. O'Connor, IEEE Trans. Magn. **2001,** 37, 2216.

22. Wang, W., Wang, D., Liu, X., Peng, Q., Li, Y., Pt-Ni nanodendrites with high hydrogenation activity. *Chem. Commun.* **2013,** *49*, 2903-2905.

23. W.H. Wang, X.L. Tian, K. Chen, G.Y. Cao, Colloid Surf. A, **2006,** 273, 35.

24. J. Solla-Gullon, A. Rodes, V. Montiel, A. Aldaz, J. Clavilier, J. Electroanal. Chem., **2003,** 554, 273.

25. K.E. Elkins, T.S. Vedantam, J.P. Liu, H. Zeng, S.H. Sun, Y. Ding, et al., Nano Lett., **2003**, 3, 1647.

26. Wang, D., Li, Y., Bimetallic Nanocrystals: Liquid-Phase Synthesis and Catalytic Applications. *Adv. Mater.* **2011,** *23*, 1044-1060.

27. Bing, Y. L., H., Zhang, L., Ghosh, D., Zhang, J., Nanostructured Pt-alloy electrocatalysts for PEM fuel cell oxygen reduction reaction. *Chemical Soc. Rev.* **2010,** *39*, 2184-2202.

28. V. K. LaMer , R. H. Dinegar , J. Am. Chem. Soc. **1950** , 72 , 4847 .

29. A. K. Sra , R. E. Schaak , J. Am. Chem. Soc. **2004** , 126 , 6667.

30. a) B. M. Leonard , N. S. P. Bhuvanesh , R. E. Schaak , J. Am. Chem. Soc. **2005** , 127 , 7326 ; b) Y. Vasquez , A. K. Sra , R. E. Schaak , J. Am. Chem. Soc. **2005** , 127 , 12504 ; c) Y. Vasquez , Z. Luo , R. E. Schaak , J. Am. Chem. Soc. **2008** , 130 , 11866 .

31. Wu, J., Zhang, J., Peng, Z., Yang, S., Wagner, F. T., Yang, H., Truncated Octahedral Pt_3Ni Oxygen Reduction Reaction Electrocatalysts. *J. Am. Chem. Soc.* **2010,** *132*, 4984-4985.

32. Liu, Q., Yan, Z., Henderson, N. L., Bauer, J. C., Goodman, D. W., Batteas, J. D., Schaak, R. E., Synthesis of CuPt Nanorod Catalysts with Tunable Lengths. *J. Am. Chem. Soc.* **2009,** *131*, 5720-5721.

33. Lim, B., Jiang, M., Camargo, P. H. C., Cho, E. C., Tao, J., Lu, X., Zhu, Y., Xia, Y., Pd-Pt Bimetallic Nanodendrites with High Activity for Oxygen Reduction. *Science* **2009,** *324*, 1302-1305.

34. Lim, B., Jiang, M., Camargo, P. H. C., Cho, E. C., Tao, J., Lu, X., Zhu, Y., Xia, Y., Shape-Controlled Synthesis of Pd Nanocrystals in Aqueous Solutions. *Adv. Funct. Mater.* **2009,** *19* (2), 189-200.

35. Wang, C., Yin, H., Chan, R., Peng, S., Dai, S., Sun, S., One-Pot Synthesis of Oleylamine Coated AuAg Alloy NPs and Their Catalysis for CO Oxidation. *Chem. Mater.* **2009,** *21*, 433-435.

36. Peng, Z., You, H., Yang, H., Composition-Dependent Formation of Platinum Silver Nanowires. *ACS Nano* **2010,** *4*, 1501-1510.

37. Schultz, M. G., Diehl, T., Brasseur, G. P., Zittel, W., Air Pollution and Climate-Forcing Impacts of a Global Hydrogen Economy. *Science* **2003,** *302*, 624-627.

38. Wolf V., H. A. G., Arnold L., *Handbook of Fuel Cells - Fundamentals, Technology and Applications*. John Wiley & Sons, Ltd.: **2003**; Vol. 2.

39. Vielstich, W., *Fuel Cells*. Wiley Interscience: New York, **1965**.

40. Metikos-Hukovic, M., Kinetics and electrocatalysis of methanol oxidation on electrodeposited Pt and Pt70Ru30 catalysts. *J. New Mater. Electrochem. Syst.* **2004,** *7*, 179-190.

Chapter 2: Synthesis and Characterization of Pt Branched Nanostructures

2.1. Introduction

Pt plays a pivotal role in many applications due to its unique physical and chemical properties.[1] Primary interests in Pt are its uses in PEMFC. For example, Pt is by far the best monometallic catalyst for methanol electrooxidation.[2,3] To improve the catalytic activity of pure Pt, one of the strategies is to increase the number of high-index facets on the Pt surface.[4] These high index planes have a high density of atomic steps, ledges, and kinks, which serve as active sites for breaking chemical bonds.[5,6] Wang and co-workers have demonstrated for the first time that the tetrahexahedra enclosed by high-index facets (e.g., {730}, {210}, and {520}) were synthesized by electrochemical treatment of Pt nanospheres. However, this approach is hard to scale up.[4] There are a number of different methods that have developed to produce Pt nanostructures including cubes, tetrahedra, octahedra, and their overgrowth structures.[7,8,9] Among these methods, the polyol synthesis is an environment-friendly approach that can control the shapes of Pt nanostructures at large-scale quantity.[10,11] In this approach, ethylene glycol, serves as a reducing agent and a solvent, while polypyrrolidone (PVP) acts as a stabilizer. A trace amount of Fe^{3+} and O_2 in the air are the oxidative etchants to retard the reduction kinetics, resulting in the overgrowth of the nanocrystals into branched and one-dimensional structures. Although this approach is proven to be a robust method to produce branched structures, the overall yield of this reaction is relatively-low and the reaction needs to be performed in a long-period of time because of the slow reduction rate. In this work, we have further developed this polyol synthesis by using a two-step mechanism involving an initial slow reduction, following by a fast reduction. Using this modified approach, the branched nanostructures can be synthesized in high yield at a shorter period of time.

2.2. Experimental

2.2.1. Materials. Dihydrogen hexachloroplatinate hexahydrate (H_2PtCl_6•$(H_2O)_6$, Alfa), polyvinylpyrrolidone (PVP 55K, M.W. = 55,000, Aldrich), hydrochloric acid (HCl, 99.9999% metal basis, Alfa), ethylene glycol (EG, J.T. Baker), polyethylene glycol (PEG, M.W. = 200, J.T. Baker), ferric chloride ($FeCl_3$, Spectrum), nitric acid (HNO_3, 99.9999% metal basis, Alfa), sodium chloride (NaCl, Alfa), citric acid ($C_6H_8O_7$, Alfa), sodium borohydride ($NaBH_4$, Alfa), polyvinylpyrrolidone (PVP 40K, M.W. = 40K, Alfa), polyvinylpyrrolidone (PVP 8K, M.W. = 8,000 Alfa), ascorbic acid (AA, EM Science), acetic acid (HAc, 99.7%, Alfa), perchloric acid ($HClO_4$, 99.9985% metal basis, Alfa), ethanol (EtOH, Koptec), and acetone ($(CH_3)_2CO$, EMD Chemicals) were used without further purification.

2.2.2. Synthesis of Pt Nanostructures. This method is a two-step procedure modified from the previous polyol synthesis reported by Chen, J. *et.al.*[10,11] In a typical synthesis, 4 mL of ethylene glycol (EG) was added to a 25-mL three-neck round-bottom flask equipped with a water-cooling condenser and heated to 110 ^oC. After 1 h, 2 mL of 32 mM $H_2PtCl_6 \cdot 6H_2O$ in EG (33 mg, 64 μmol), 2 mL of polyvinylpyrrolidone in EG (PVP, M.W.=55,000, 0.045 g) were simultaneously added to the EG, followed by adding 0.1 mL of 200 mM $FeCl_3$ in EG, 0.5 mL of 6 mM HCl in EG, and 2 mL of 32 mM of $CuCl_2$ (8.5 mg, 63 μmol) in EG. The reaction mixture was then maintained at 110 ^oC for a certain period of time varying from 2 to 24 h. The color of the reaction was changed from golden yellow to green yellow, indicating the reduction of Pt precursor. After this initial period of slow reduction, 0.5 mL of 500 mM of ascorbic acid was added to the reaction mixture to introduce a fast reduction as a second step. Within 15 min, the color of the reaction mixture was changed from green yellow to dark brown, indicating the formation of nanoparticles. The product was then precipitated out by 5 times of acetone and centrifugation, followed by washing twice with ethanol. The final pellet was suspended in 18 Ω water for further use.

To study the role of HCl, all parameters of the synthesis were kept the same except that an additional solution was injected to the reaction at the stage of the addition of H_2PtCl_6, PVP 55K, and $FeCl_3$ solutions. Four different syntheses were performed with the addition of 50 μL of 5.285 mM HCl, 50 μL of 18 Ω water, 50 μL of 5.285 mM NaCl, and 50 μL of 5.285 mM HNO_3, respectively.

For the time course study of the slow reduction, all parameters of the synthesis were kept the same except that the reaction time for the slow reduction step varied from 2, to 5, 10, 15, 20, 45, 60, 720, and 1080 min.

To study the reducing power of the reducing agent, all parameters of the synthesis were kept the same except that different reducing agents were used in the second step including citric acid (50 mM) in 0.5 mL EG, $NaBH_4$ (100 mM) in 0.5 mL EG, and $NaBH_4$ (5 mM) in 0.5 mL EG, respectively.

To study the effect of oxygen, all parameters of the synthesis were kept the same except that the reaction was performed under argon.

To further separate the individual branched nanostructures from the large agglomerates, the product was centrifuged at 5,500 rcf for 10 min. The supernatant contains the branched nanostructures and the precipitate contains the large agglomerates.

2.2.3. Instrumentation. TEM images were taken on a JEOL 100 CX electron microscope using a 100 kV accelerating voltage. The sample was prepared by dropping 5 μL of nanoparticle aqueous suspension on a formvar-coated copper grid. The grid was dried in air either held by a self-closed tweezers or on filter paper. X-ray diffraction (XRD) patterns were acquired using a Rigaku MiniFlex X-ray diffractometer equipped with Cu Kα radiation source operated at 30 kV/15 mA. The concentrations of Pt and other metals were determined using a GBC 932 atomic absorption spectrometer (AAS). An aliquot (200 μL) of nanoparticle suspension was digested

with aqua regia (3:1 v/v ratio of HCl and HNO_3) before dilution in the matrix for the AAS measurement. The calibration curve was used to determine the concentration of Pt nanoparticle sample. UV-vis spectra were taken on an HP 8453 UV-visible spectrophotometer.

2.2.4. Electrocatalytic Activity of Pt Nanostructures. The electrocatalytic activity of the Pt-Cu nanodendrites and commercial Pt/C (20 wt%) catalysts were characterized by cyclic voltammetry (CV) and chronoamperometry (CA) on a CHI760 electrochemical workstation at room temperature. The measurements were performed using a three-electrode cell with the Ag/AgCl/1.0 M KCl electrode (E^o = -0.294 V vs. RHE) and Pt wire as reference and counter electrode, respectively. Glassy carbon disk (0.070 cm^2) was polished to a mirror finish before each experiment and was used as substrate for the working electrode. The catalyst suspension was prepared by mixing 1:1 volume of 0.4 mg_{Pt}/mL nanoparticle suspension with 0.05 wt% Nafion, followed by sonicating for 5 min. A 5 μL aliquot of the suspension was pipetted onto the glassy carbon substrate, yielding a Pt loading of 2 μg or 28 μg/cm^2. The working electrode was dried at room temperature. The electrochemical active surface area (ECSA) was determined from CV profile obtained at a scan rate of 50 mV/s in 0.1 M $HClO_4$ solution. The methanol oxidation was carried out in a solution containing 1.0 M CH_3OH and 0.1 M $HClO_4$ at a scan rate of 50 mV/s. The CA was recorded at 0.9 V vs. RHE in a solution containing 1.0 M CH_3OH and 0.1 M $HClO_4$. The electrochemical dealloying process was carried out at a scan rate of 50 mV/s with the potential range from 0 to 1.2 V vs. RHE in 0.1 M $HClO_4$ solution. After a certain number of cycles, the CV profile was recorded at a scan rate of 50 mV/s.

2.3. Results and Discussion

2.3.1. Synthesis

Figure 2-1 illustrates the over strategy of the two-step process involving a slow reduction by EG and a fast reduction by AA. In the first step, EG, a very mild reducing agent, allows for a slow

reduction Pt(IV) ions to Pt(II) ions. During the preheating process, EG was oxidized by air to generate a small amount of glycolaldehyde (GA).[12]

$$2HOCH_2CH_2OH + O_2 \rightarrow 2HOCH_2CHO + 2H_2O \quad (1)$$

The Pt(IV) precursor was reduced by GA to Pt(II) ions and Pt(0).[11] The reduction kinetics was

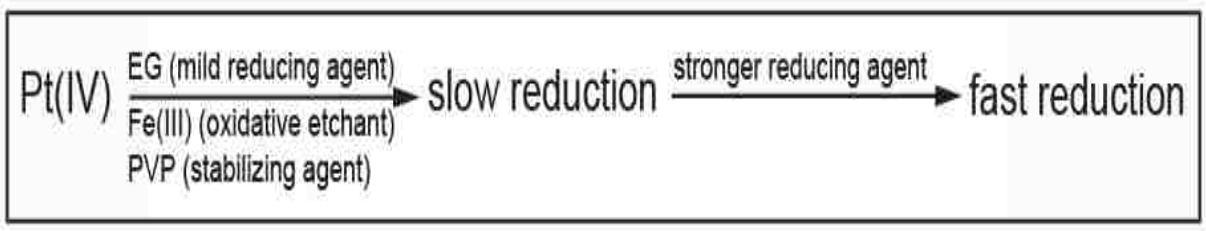

Figure 2-1. Schematic illustration of the overall strategy for the synthesis of Pt nanostructures via a two-step reduction process.

controlled by adding a trace amount of Fe(III), which could oxidize the Pt(0) back to Pt(II).[10] This oxidative agent combined with the capping agent PVP 55K could eliminate the twinned seed and activate the {111} facets for overgrowth. In the second step, AA was used as a reducing agent for rapidly reducing the precursors on the activated seeds for overgrowth in a short-period of time. The overgrowth of the single-crystalline seeds leads to a high yield of branch nanostructures. The effects of each parameter on synthesis will be discussed in the following subsections.

2.3.1.1. Slow Reduction Step

The slow reduction is the key step to induce the overgrowth of single-crystalline seeds for the formation of branched nanostructures. The retardation of the reduction kinetics is controlled by Fe (III)/Fe(II) ion redox species and oxygen in the air. In order to determine the optimal time for the slow reduction process we performed a time-course study at which a stronger reducing agent was added to complete the reaction, Figure 2-2 shows TEM images of the branched nanostructures. Samples, A-I, were prepared by slowly reducing in EG at 110 °C followed by fast reducing by AA at a final concentration of 3.84 mM for 30 min. At short slow reduction

periods (≤ 60 min.) the final products were star-shaped. As the slow reduction time extended to 12 h the nanoparticle started to branch out a little more and coalescence. Figure 2-3 shows a

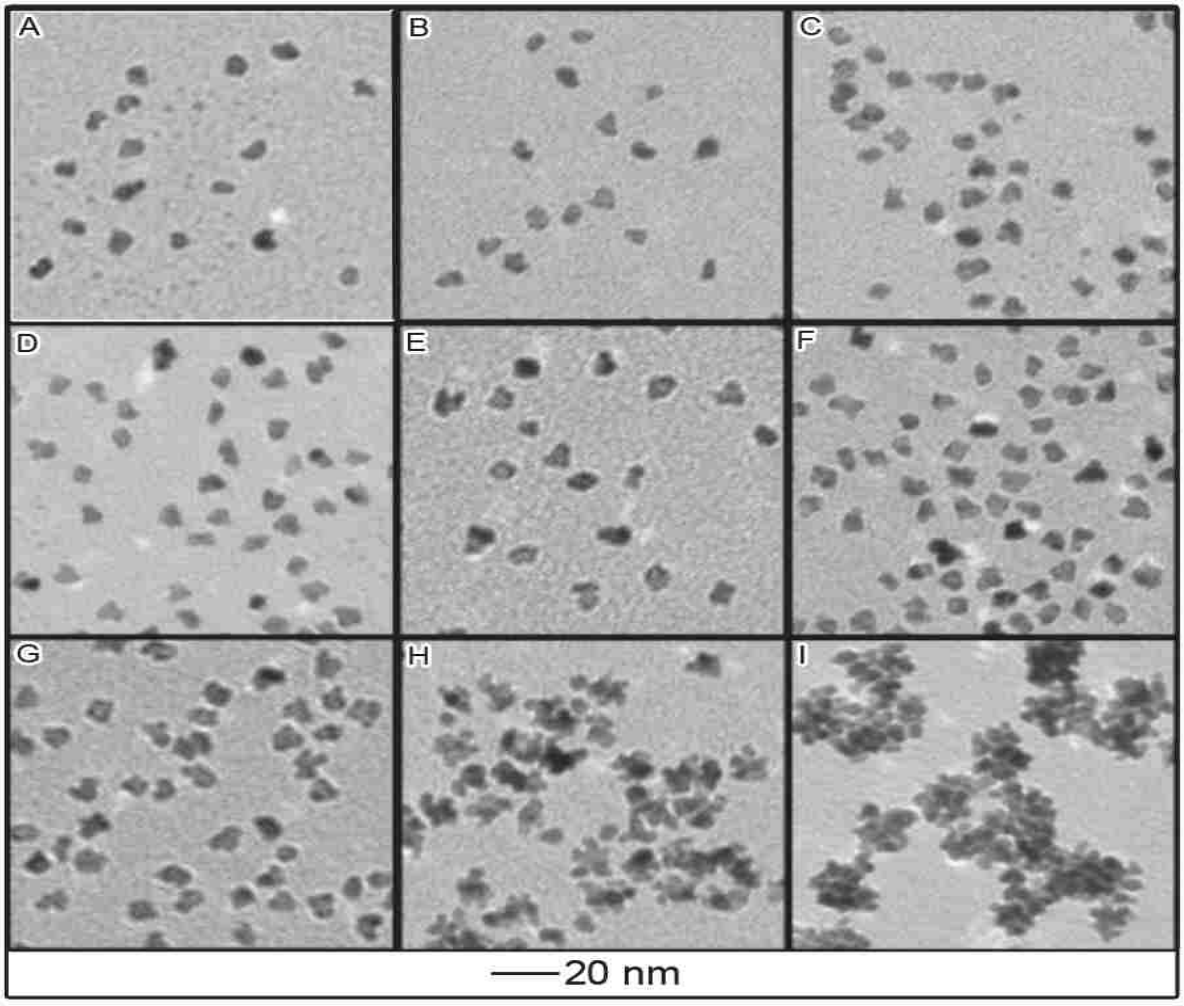

Figure 2-2. TEM images of the samples synthesized by reducing in EG at different time periods followed by fast reducing in AA for 30 min: ***(A)*** *2;* ***(B)*** *5;* ***(C)*** *10;* ***(D)*** *15;* ***(E)*** *20;* ***(F)*** *45;* ***(G)*** *60;* ***(H)*** *720; and* ***(I)*** *1080 min.*

time course study for the slow reduction step using UV-vis spectroscopy. Previous studies have shown that the presence of Pt(IV), Pt(II), and Pt(0) species can be monitored using UV-vis.[11] The peak at 267 nm can be assigned to Pt(IV), while the peak at 247 nm is associated with Pt(II).[13] During the slow reduction step the concentration of Pt(0) is very low therefore there is no detectable peak for Pt(0) in this case.[10] The absorbance of Pt(IV) experienced decreases dramatically at one hour this is accompanied with the rise of the peak at 247 nm indicating that

most of the Pt(IV) was reduced to Pt(II) within an hour. After that, the concentration of Pt(IV) remains low while the concentration of Pt(II) deceases to a plateau at 4 hr. At this time, the reaction solution was still a golden color and not any shade of brown which indicates the production of Pt(0) nanostructures was very low.[10]

To elongate the branches of the nanoparticles the reaction conditions of the slow reductions step needs to be altered by retarding the kinetics as suggested in the previous study. [14] Various conditions were examined to find out the key parameter for the production of branched nanostructures. It has been shown that the reducing power of the reactant and/or trace amounts of an oxidating agent can have a significant on the nanostructure.[9, 10] For these reactions PEG was chosen to replace EG as a reducing agent and solvent because PEG has fewer –OH groups available as compared to EG at the same amount of solvent. Note that the viscosity of the reaction solution increased with increasing the chain length of the polymer.[15] Figure 2-4 shows that the product is

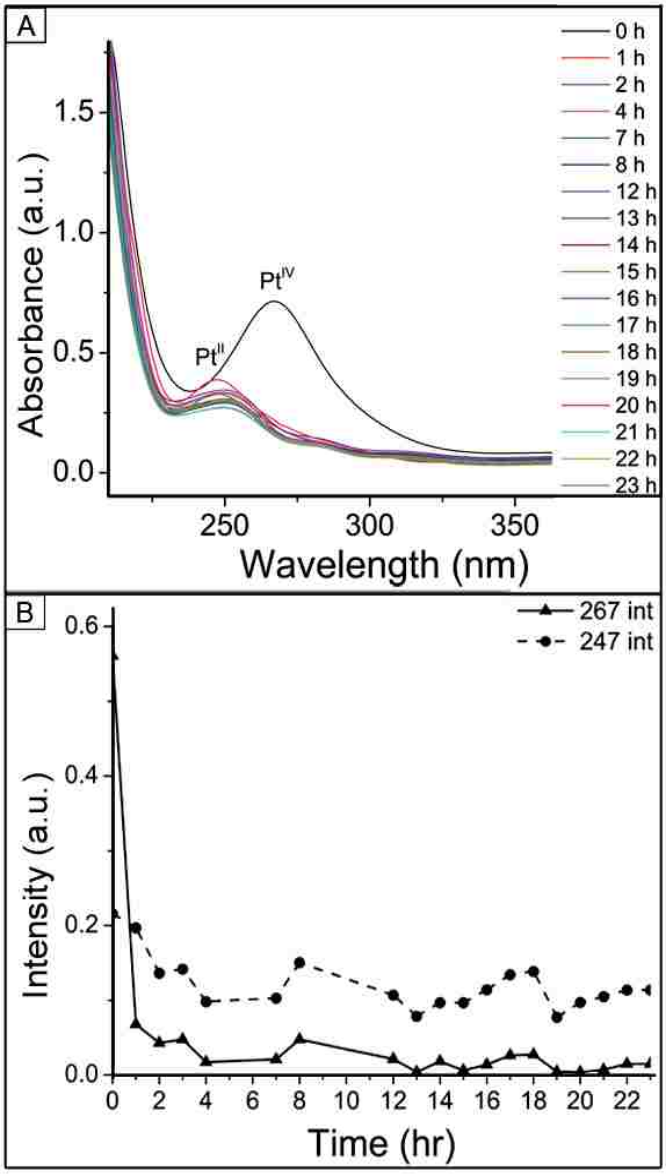

Figure 2-3. **(A)** *UV-vis spectra of sample aliquots taken from the reaction at different time points.* **(B)** *Plot of peak intensity as a function of time at 267 nm (Pt(IV)) and 247 nm (Pt(II)) respectively.*

more branched out than the previous ones. Further extension of the reduction time led from 24 h to 54 h. The overgrowth of the branched structures led to large aggregates of Pt seen in Figure 2-4 B. The cause for overgrowth is a low concentration of Pt seeds and a high concentration of free Pt ions loose in solution.[7]

Trace amounts of substances in the reaction affects the morphology of the final products. Several factors were considered to play a role in the slow reduction of the branched structures. The addition of HCl produced highly branched nanostructures (Fig. 2-5A) while the addition of water generated clumps of particles (Fig. 2-5B). In order to determine the role of Cl^- and H^+ ions two more reactions were performed by replacing the HCl with NaCl (source of Cl^-) and HNO_3 (source of H^+). In bithe cases, there were some branched particles present in the product, but at a low yield. Therefore we concluded that both Cl^- and H^+ ions influence the reduction kinetics to generate the dect sites for overgrowth. If the twinned seeds are present, then the atoms in these outer grow boundaries are more susceptible to oxidative etching than the single crystal seeds.[14] As a result, HCl tunes the crystallinity of the seeds from twinned to single crystals. On the other hand, the HCl etching slows down the rate of atomic addition.[16] At the same time, HCl activates the {111} facets in the single crystal seed for overgrowth resulting in the growth along the axis of the [111] plane of the

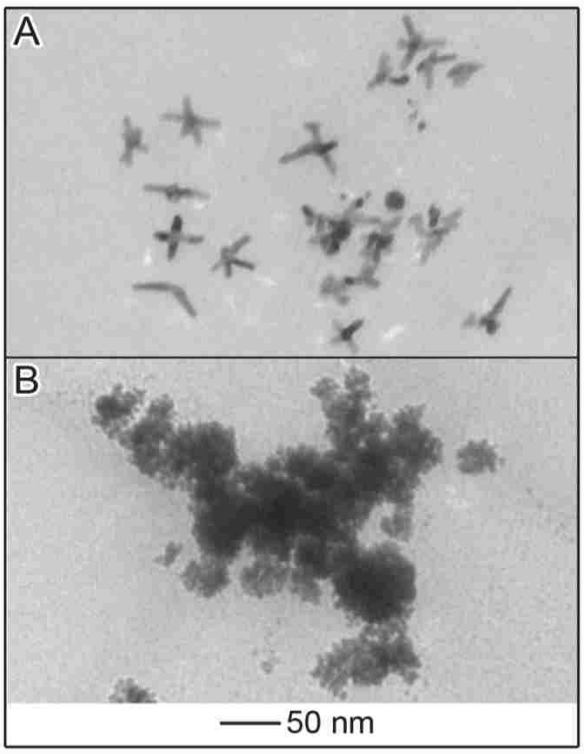

Figure 2-4. TEM images of Pt nanostructures synthesized by the two-step synthesis in PEG at different slow nucleation times, **(A)** *24 and* **(B)** *54 hours.*

single crystals. As the concentration increases, the number of [111] overgrowth branches increases resulting in different number of branches.[17]

2.3.1.2. Fast Reduction Step

We have examined the factors in the fast reduction step including the concentration and the type of the secondary reducing agent. To study the effect of concentrations a series of experiments were conducted at different time periods after the injection of the 0.5 mL of 500 mM AA, (Fig. 2-6 A-C), 30, 15 and 12 min., respectively. The experiment results showed that 15 min. is the optimal time for the fast reduction step that produced the longest and mostly uniform branched nanostructures. At the optimal condition of the fast reduction step we examined the slow reduction step for 12 h (Fig. 2-6D). To examine whether the reduction kinetics has an effect

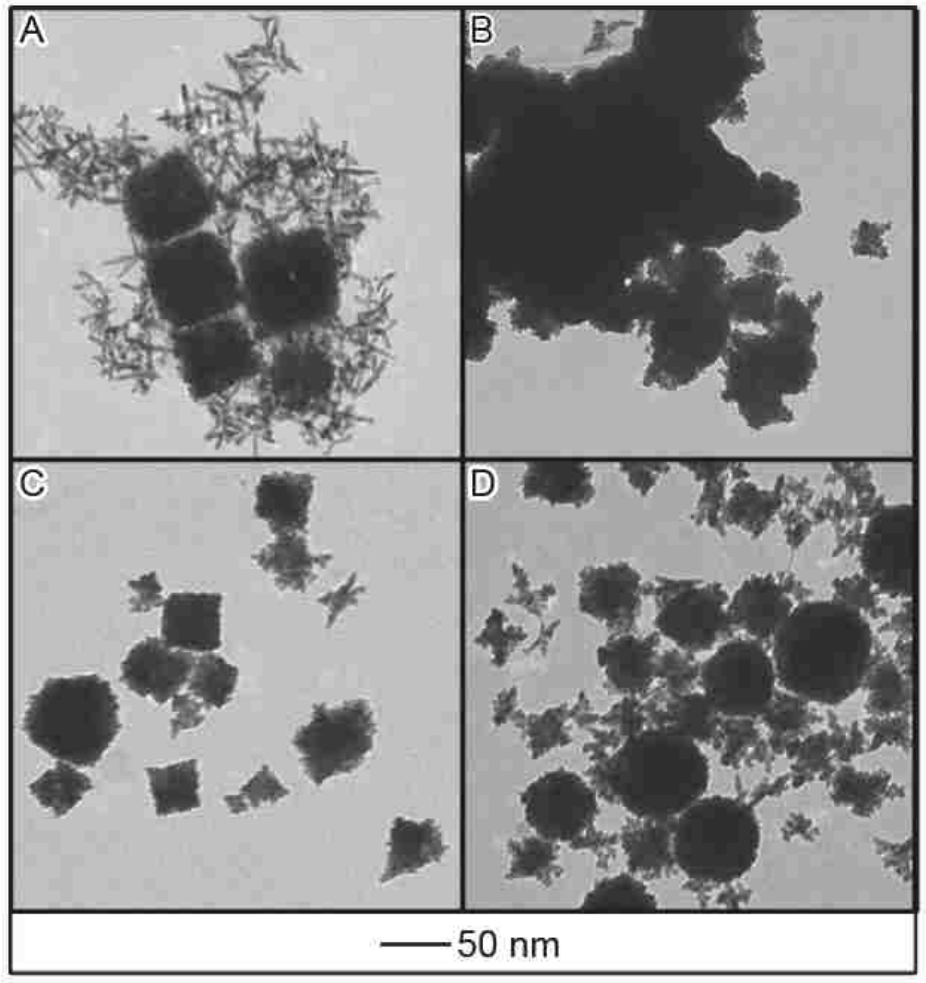

Figure 2-5. TEM images of Pt nanostructures synthesized by adding a small amount of additives in the two-step procedure. **(A)** *HCl (5.285 mM in 50 μL),* **(B)** *H_2O (50μL),* **(C)** *NaCl(5.285 mM in 50μL), and* **(D)** *HNO_3(5.285 mM in 50μL).*

on the final shape of the nanoparticle different reducing agents were compared in the fast step reduction.[18, 19, 20] The relative reducing power of these reducing agents are citric acid < ascorbic acid < $NaBH_4$ 5 mM < $NaBH_4$ 500 mM.[21] Figure 2-7, A-D, shows the TEM images of the

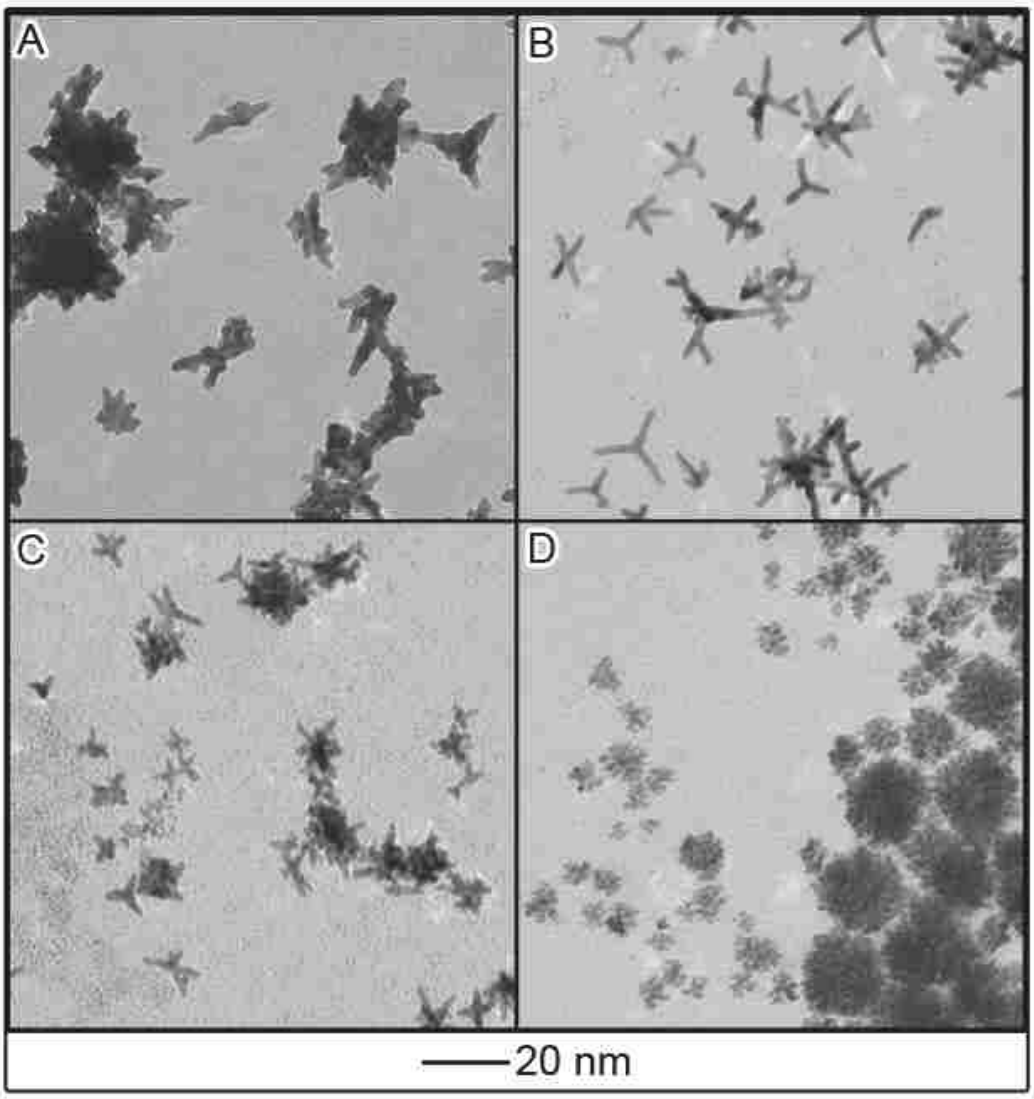

Figure 2-6. TEM images of Pt nanostructures synthesized by maintaining the slow reduction step at 24 hours and changing the fast reduction time in the two-step procedure, **(A)** *30,* **(B)** *15, and* **(C)** *12 min.* **(D)** *Fast reduction step at 12 h and slow reduction step at 15 min.*

resultant products form these syntheses. When AA is used as the reducing agent, the color of the reaction mixture turns from green yellow to dark brown within the 15 min. However, when using citric acid, the color of the solution starts as a green yellow color and turns a light brown/grey

color within fifteen minutes. The darker the color the more concentrated the sample platinum concentration is. The small particles tend to appear as a brown color while the branched particles

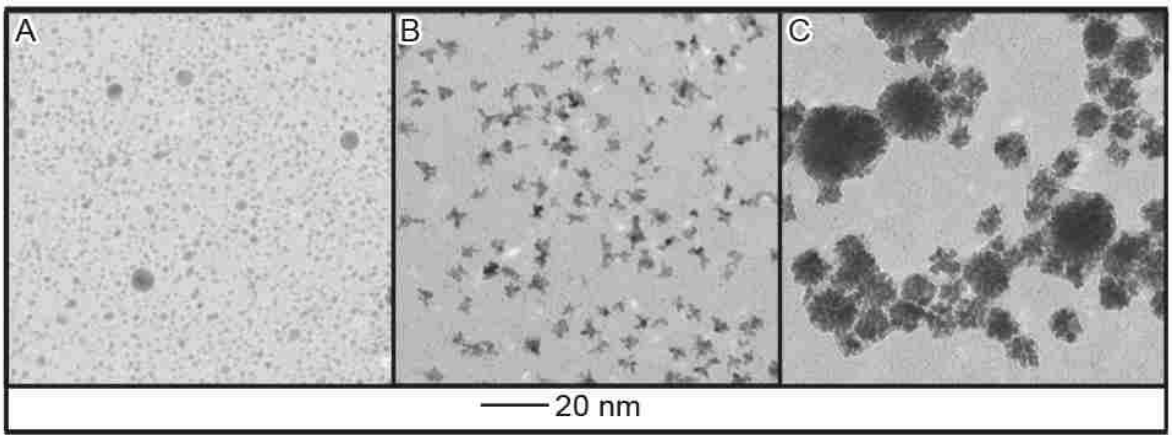

Figure 2-7. TEM images of Pt nanostructures synthesized by the two-step procedure using different reducing agents in the fast reduction step. **(A)** *0.5 mL of 50 mM citric acid,* **(B)** *0.5 mL of 5 mM $NaBH_4$, and* **(C)** *0.5 mM of 500 mM $NaBH_4$.*

or agglomerates become black. The results are in agreement to the reducing power of each reducing agent. In the case of citric acid it is a weaker reducing agent as compared to AA as a result less Pt(0) was observed at the same reduction time. As a result, most of the product remains to be small particles, Figure 2-7A.[14] We also examined a stronger reducing agent (e.g. $NaBH_4$). The morphology of the final product depends on the concentration of the $NaBH_4$. At low concentrations the reducing power of the agent is comparable to that of the AA nanoparticles which short branches were found (Fig. 2-7B). At high concentrations larger agglomerates were formed due to the coalescence of particles at very high concentrations (Fig. 2-7C). [20]

2.3.1.3. Other Considerations

We further investigated the effects of other parameters on the shape of the product in this synthesis. It is known that the capping agent plays a role in controlling the shapes of the particles.[8] The lone pair electrons on the N and O of PVP were previously found to bond to the surface of Pt.[22, 23] We hypothesized that the chain length of the PVP could affect the shape of the particles. [24] To test this hypothesis different chain lengths of PVP (i.e. PVP 40K and PVP 8K)

were used to replace the PVP 55K in this synthesis. Figure 2-8A and B shows the TEM images of the resultant products. The reaction with 44K PVP yielded nanoparticles with long branches along with some big agglomerates, while the reaction with 8K generated only ultra-small star-shaped nanoparticles. This result is possibly due to the difference in both viscosity and interaction with particle surface. By lowering the MW of the PVP, this decreased the length of the polymer chain protecting the surface of the seeds, resulting in the formation of smaller particles. At the same time, the longer PVP chain is more viscous, thereby slowing down the reduction kinetics of the Pt ions.[8] The PVP with longer chain length may be less rigid in solution. When bound to the surface of Pt seeds, some of the facets (i.e. {111}) are exposed for deposition of the reduced Pt(0) atoms allowing the overgrowth along the <111> axis.[25]

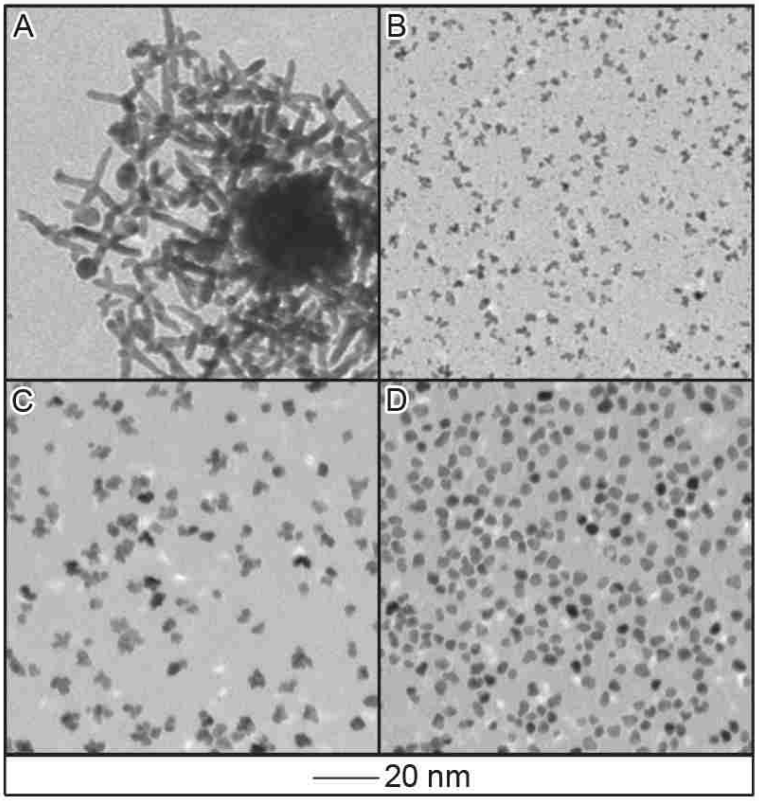

Figure 2-8. TEM images of Pt nanostructures synthesized by the two-step procedure using different PVP MW in the fast reduction step, **(A)** *40K and* **(B)** *8K. TEM images of Pt nanostructures synthesized by the two-step procedure using different PVP MW in the fast reduction step in an argon atmosphere,* **(C)** *40K and* **(C)** *8K.*

Previous studies have found that oxygen could be an oxidative etchant of Pt(0) for controlling the reduction kinetics.[26] We then examined the effect of oxygen in this modified synthesis. The reactions were performed under an argon atmosphere. As shown in Figure 2-8, C

and D, only ultra-small particles were found in both reactions.[10] Clearly, oxygen plays a major role in the generation of branched nanostructures by slowing down the reduction rate of Pt(0).[8]

Another oxidative agent, FeCl3, was examined for controlling the shape of the nanoparticles.[11] Without the addition of the Fe(III) species, the Pt(II) species reduces to Pt(0) much faster within a few hours to form spherical Pt nanoparticles autocatalytically. The Fe(III) species oxidizes the Pt(0) species back to Pt(II) which will reduce the supersaturation of Pt atoms in the solution and lower the likelihood of autocatalytic reduction occurring. If the concentration of the Fe(III) is high enough, the reduction of Pt(II) halts and Pt(0) nanostructures will not form autocatalytically for several weeks.[27] The concentration of $FeCl_3$ is critical in producing branched nanoparticles in the synthesis. For example, when lower concentrations (i.e. 50 mM and 100 mM) were used within the reactions no highly branched particles were formed.

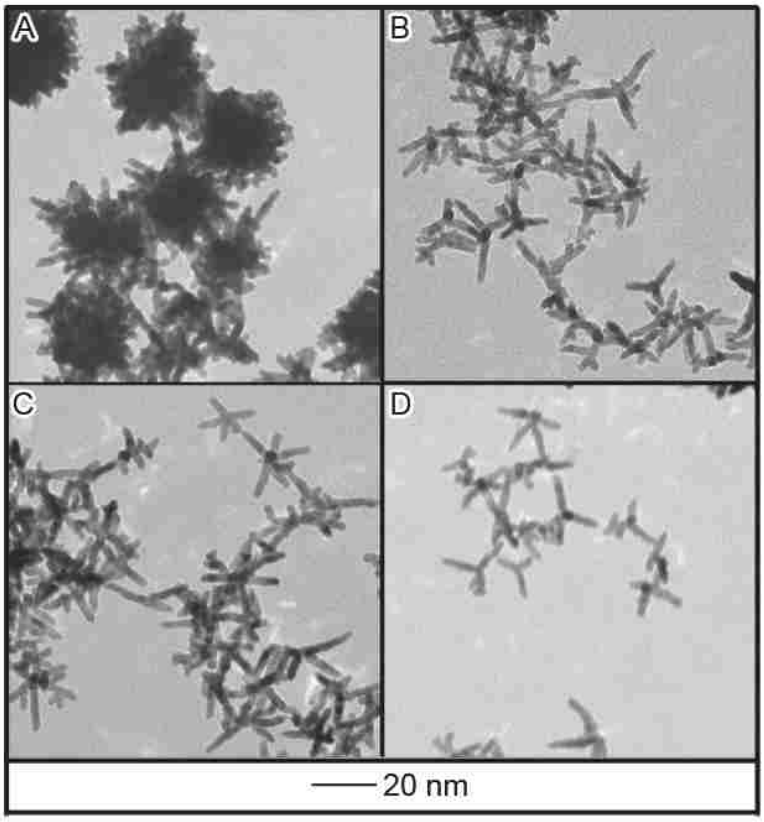

Figure 2-9. Separating aggregates by centrifugation, **(A)** *pellet and* **(B)** *supernatant. TEM sample preparation using different drying techniques,* **(C)** *tweezers and* **(D)** *filter paper.*

In a typical synthesis there are aggregates present in the products. To separate the aggregates from the isolated nanoparticles a centrifugation method was used. [28,29] This separation method is based on the mass difference between the two types of particles. At a slow

centrifugation speed nanoparticles with higher mass (i.e. aggregates) precipitate out of solution more easily than that of the lower mass (i.e. branched) nanoparticles. As a result the branched nanoparticles can be separated from the agglomerates remaining in the supernatant (Fig 2-9A). The pellet only contained large agglomerates while the supernatant was dominated by individual nanoparticles (Fig. 2-9B). After the product was centrifuged at 5500 rpm for 10 min. During the drying process on the grid the branched nanoparticles were self-assembled as a "spider web" like island due to the surface tension of water. These may reflect the morphology on the electrode surface after the drying process. To prove that the "spider web" shape is the assembly of isolated branched particles different sample preparation processes were used. Figure 2-9, C and D, show the samples prepared by drop casting on a TEM grid held by self-closing tweezers and by placing the grid on filter paper, respectively. The fast drying process on the filter paper should prevent the stacking of the nanoparticles if they are isolated particles. The result clearly indicated that the particles from the synthesis were made of individual branched particles (Fig. 2-9D) and were stacking while drying and had not grown together.

2.3.2. Evaluation of Electrocatalytic Activity

The electrochemical activity of the Pt nanostructure was evaluated by the methanol oxidation half reaction. The samples were concentrated to 0.8 $mg_{(Pt)}$ / mL and the Pt/C was used as a standard at the same concentration. Each 0.8$mg_{(Pt)}$ / mL sample was diluted with Nafion to obtain a final concentration of 0.4$mg_{(Pt)}$ / mL. Nafion is used as a conductive polymer that prevents the particles from coming off the electrode surface. [30] Half of the each branched particle samples was treated by and acetic acid (mixture of 5:1 v/v nanostructures: 50% acetic acid, for 3 h at 60 °C) to remove the surface ligand, PVP. Preliminary results had concluded that an excess of PVP on the surface of the nanostructures reduced the amount of current observed. A CV profile of each sample was obtained by sweeping from -0.4 to -0.906 V (vs. Ag/AgCl in 1M

KCl) at a scan rate of 50 mV/s in 0.1 M $HClO_4$ (Fig. 2-10A). The hydrogen desorption area between -0.24 to 0.0406 V (vs. Ag/AgCl in 1M KCl) was integrated and used to calculate the

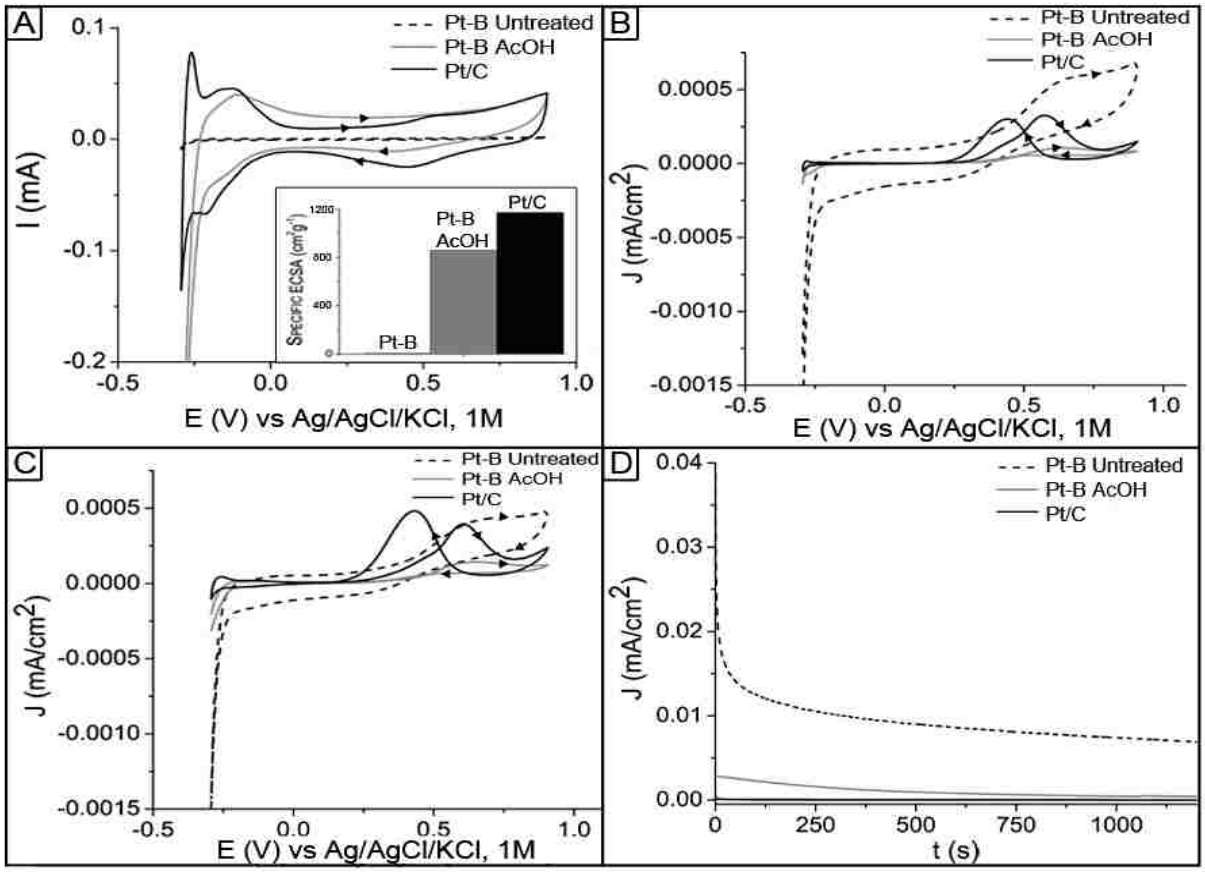

Figure 2-11. Electrochemical measurements of Pt alloyed nanostructures before acetic acid treatment. **(A)** *Cyclic voltammetric (CV) profiles in a 0.1 M $HClO_4$ solution at 50 mV/s, inset is the plot of the specific electrochemical surface area for the specific alloy ratios from left to right, 5.65, 859.84, 1170.67 cm^2.* **(B-C)** C*yclic voltammetric and* **(D)** *Chronoamperometry (CA) results of MOR in a 0.1 M $HClO_4$ and 1 MeOH solution at* **(B)** *10 mV/s and* **(C)** *50 mV/s. CA curves were recorded at 1V vs. Ag/AgCl/KCl, 1M.*

electrochemical surface area (ECSA). The ECSA of each sample was plotted in the inset of Fig. 2-10A. The results indicate that the ECSA of the acetic acid branched nanoparticles >> untreated particles. This suggested the excess PVP coverage on the electrode largely reduced the conductivity of the particles thereby lowering the current observed. For comparison, current density (current/ECSA) was calculated and plotted as a function of potential for methanol oxidation reaction (MOR). Because the untreated sample has extremely low surface area it was

misleading to use the data for calculations of the ECSA. Therefore, we only compared the treated samples with Pt/C. For Figure 2-10 Pt-B untreated, Pt-B HAc, and Pt/C referred to untreated Pt branched nanoparticles, acetic acid treated Pt branched nanoparticles and carbon-supported Pt nanoparticles, respectively. Figure 2-10, B and C, show the current density versus potential at the different scan rates at 10 mV/s and 50 mV/s, respectively. The I_f/I_b ratio was calculated to be xx and xx for Pt-B HAc and Pt/C at a scan rate of 10 mV/s, respectively and xx and xx for Pt-B HAc and Pt/C at a scan rate of 50 mV/s, respectively. In both cases , the ratio of (I_f/I_b) of Pt-B HAc is higher than that of the Pt/C. It is implied that the Pt-B HAc could resist the poisoning of CO like intermediates.[31] The positioning decreased with increased scan rate. The results are possible due to the presence of higher index facets in the Pt branched nanostructures. The chronoamperometry was also measures by plotting the current density as a function of time at 1V (vs. Ag/AgCl in 1M KCl). The result suggested that the Pt-B HAc was more stable than the Pt/C.

2.4. Conclusion

A two-step procedure synthesis was developed to successfully generate branched Pt nanostructures in a reasonably-high yield. In the slow step, the presence of oxidative etchants such as Fe(III), Cl^-, and O_2, are essential to obtain the single-crystalline seeds with {111} facets activated for overgrowth. In the second step, a stronger reducing agent, AA, was used to introduce a fast reduction process to shorten the reaction time and produce the branched nanostructure in high yield. The large agglomerates in the product could be removed from the product by centrifugation. The Pt branched nanostructures were studied for their electrochemical activity as a catalyst for MOR. As compared to the commercially-available Pt/C, the Pt branched nanostructures have a lower normalized ECSA/g_{Pt} possibly due to the lack of carbon support and the presence of agglomeration of the Pt nanostructures. The Pt branched nanostructures exhibit less poisoning by CO_{ad} species from MOR possibly due to the presence of more active sites as

compared to the Pt nanoparticles. Further analysis of the nanostructures is needed.

2. 5. References

1. Gasteiger, H. A., Kocha, S. S., Sompalli, B., Wagner, F. T., Activity benchmarks and requirements for Pt, Pt-alloy, and non-Pt oxygen reduction catalysts for PEMFCs. *App. Catal., B* **2005,** *56*, 9-35.

2. Wolf V., H. A. G., Arnold L., *Handbook of Fuel Cells - Fundamentals, Technology and Applications*. John Wiley & Sons, Ltd.: **2003**; Vol. 2.

3. Formo, E., Peng, Z., Lee, E., Lu, X., Yang, H., Xia, Y., Direct Oxidation of Methanol on Pt Nanostructures Supported on Electrospun Nanofibers of Anatase. *J. Phys. Chem. C.* **2008,** *112*, 9970-9975.

4. Tian, N., Synthesis of Tetrahexahedral Platinum Nanocrystals with High-Index Facets and High Electro-Oxidation Activity. *Science* **2007,** *316*, 732-735.

5. Somorjai, G. A., Blakely, D.W., Mechanism of catalysis of hydrocarbon reactions by platinum surfaces. *Nature* **1975,** *258*, 580 -583.

6. Sun, S. G., Chen, A. C., Huang, T. S., Li, J. B., Tian, Z. W., Electrocatalytic properties of Pt(111), Pt(332), Pt(331) and Pt(110) single crystal electrodes towards ethylene glycol oxidation in sulphuric acid solutions. *Journal of Electroanalytical Chemistry* **1992,** *340*, 213-226.

7. Chen, J., Lim, B., Lee, E. P., Xia, Y., Shape-controlled synthesis of platinum nanocrystals for catalytic and electrocatalytic applications. *Nano Today* **2009,** *4*, 81-95.

8. Ahmadi, T. S., Wang, Z. L., Green, T. C., Henglein, A., El-Sayed, M. A., Shape-Controlled Synthesis of Colloidal Platinum Nanoparticles. *Science* **1996,** *272*, 1924-1925.

9. Xiong, Y. e. a., Control Over the Branched Structures of Platinum Nanocrystals for Electrocatalytic Applications. *ACS Nano* **2012,** *6*, 9797-9806.

10. Chen, J., Herricks, T., Xia, Y., Polyol Synthesis of Platinum Nanostructures: Control of Morphology through the Manipulation of Reduction Kinetics. *Angew. Chem. Int. Ed.* **2005,** *44*, 2589-2592.

11. Chen, J., Herricks, T., Geissler, M., Xia, Y., Single-Crystal Nanowires of Platinum Can Be Synthesized by Controlling the Reaction Rate of a Polyol Process. *J. Am. Chem. Soc.* **2004,** *126*, 10854-10855.

12. Skrabalak, S. E., Wiley, B. J., Kim, M., Formo, E. V., Xia, Y., On the Polyol Synthesis of Silver Nanostructures: Glycolaldehyde as a Reducing Agent. *Nano Letters* **2008,** *8*, 2077-2081.

13. Herricks, T., Chen, J., Xia, Y., Polyol Synthesis of Platinum Nanoparticles: Control of Morphology with Sodium Nitrate. *Nano Lett.* **2004,** *4*, 2367-2371.

14. Wang, D., Li, Y., Bimetallic Nanocrystals: Liquid-Phase Synthesis and Catalytic Applications. *Adv. Mater.* **2011,** *23*, 1044-1060.

15. Gonzalez-Tello, P., Camacho, F., Blazquez, G., Density and Viscosity of Concentrated Aqueous Solutions of Polyethylene Glycol. *J. Chem. Eng. Data* **1994,** *39*, 611-614.

16. Xiong, Y. e. a., Size-Dependence of Surface Plasmon Resonance and Oxidation for Pd Nanocubes Synthesized via a Seed Etching Process. *Nano Letters* **2005,** *5*, 1237-1242.

17. Teng, X., Yang, H., Synthesis of Platinum Multipods: An Induced Anisotropic Growth. *Nano Letters* **2005,** *5*, 885-891.

18. Lim, B., Jiang, M., Camargo, P. H. C., Cho, E. C., Tao, J., Lu, X., Zhu, Y., Xia, Y., Shape-Controlled Synthesis of Pd Nanocrystals in Aqueous Solutions. *Adv. Funct. Mater.* **2009,** *19* (2), 189-200.

19. Chen, J.; Wiley, B. J.; Xia, Y., One-Dimensional Nanostructures of Metals: Large-Scale Synthesis and Some Potential Applications. *Langmuir* **2007,** *23* (8), 4120-4129.

20. Jiang, M., Lim, B., Tao, J., Camargo, P. H. C., Ma, C., Zhu, Y. Xia, Y., Epitaxial overgrowth of platinum on palladium nanocrystals. *Nanoscale* **2010,** *2*, 2406-2411.

21. Hussain, J., Kumar, S, Hashmi, AA, Khan, Z, Silver nanoparticles: preparation, characterization, and kinetics. *Adv. Mat. Lett.* **2011,** *2*, 188-194.

22. Yin, B., Ma, H., Wang, S., Chen, S., Electrochemical Synthesis of Silver Nanoparticles under Protection of Poly(N-vinylpyrrolidone). *J. Phys. Chem. B* **2003,** *107*, 8898-8904.

23. Zhu, J. J., Kan, C., Wan, J. G., Han, M., Wang, G. H., High-Yield Synthesis of Uniform Ag Nanowires with High Aspect Ratios by Introducing the Long-Chain PVP in an Improved Polyol Process. *J. Nano. Mater.* **2011,** *20111*, 1-7.

24. Swei, J., Talbot, J. B., Viscosity correlation for aqueous polyvinylpyrrolidone (PVP) solutions. *J. App. Polym. Sci.* **2003,** *90*, 1153-1155.

25. Chen, Z., Yan, Y., Supportless Pt and PtPd Nanotubes as Electrocatalysts for Oxygen-Reduction Reactions. *Angew. Chem. Int. Ed.* **2007,** *46*, 4060-4063.

26. Mallat, T. B., A., Oxidation of alcohols with molecular oxygen on platinum metal catalysts in aqueous solutions. *Catal. Today* **1994,** *19*, 247-283.

27. Chen, J. H., T. Xia, Y., Polyol Synthesis of Platinum Nanostructures: Control of Morphology through the Manipulation of Reduction Kinetics. *Angew. Chem. Int. Ed.* **2005,** *44*, 2589-2592.

28. Akbulut, O., Mace, C. R., Martinez, R. V., Kumar, A. A., Nie, Z., Patton, M. R., Whitesides, G. M., Separation of Nanoparticles in Aqueous Multiphase Systems through Centrifugation. *Nano Letters* **2012,** *12*, 4060-4064.

29. Kowalczyk, B., Lagzi, I., Grzybowski, B. A., Nanoseparations: Strategies for size and/or shape-selective purification of nanoparticles. *Curr. Opin. Colloid Interface Sci.* **2011,** *16*, 14-14.

30. Mauritz, K. A., Moore, R. B., State of Understanding of Nafion. *Chem. Rev.* **2004,** *104*, 4535-4586.

31. Papadimitriou, S.; Armyanov, S.; Valova, E.; Hubin, A.; Steenhaut, O.; Pavlidou, E.; Kokkinidis, G.; Sotiropoulos, S., Methanol Oxidation at Pt−Cu, Pt−Ni, and Pt−Co Electrode Coatings Prepared by a Galvanic Replacement Process. *The Journal of Physical Chemistry C* **2010,** *114* (11), 5217-5223.

Chapter 3: Synthesis and Characterization of Pt-Cu Dendritic Nanoparticles

3.1. Introduction

Platinum-containing bimetallic nanostructures are attractive for many applications, in particular, heterogeneous catalysis. For example, Pt-Cu alloyed nanoparticles have been predicted as bifunctional catalysts to improve the methanol oxidation. In this case, Pt is the best known monometallic catalyst that can activate the methanol molecule, while Cu is an excellent catalyst for oxidation reactions.[1] The combination of the two elements in the alloy can synergistically activate CO on Pt and OH on Cu, thereby effectively oxidizing the CO-like molecules into CO_2 to avoid the poisoning of the catalyst. On the other hand, the Cu can alter the electronic structure of Pt to promote the complete oxidation reaction. The efficiency of the improvement depends on the atomic arrangement in the alloy. A few examples has been shown that the catalytic activity of the Pt-Cu alloyed nanoparticles is dictated by their morphology such as nanocubes,[2] hollow nanoparticles,[3] nanocages,[4] nanorods,[5] and core-shell.[6] Recent studies showed that the nanodendritic structures contain rich amount of active sites on their surface and they exhibit high activity for electrocatalysis of ORR and FAOR.[7,8] In this work, we have developed a co-reduction method to synthesize the Pt-Cu nanodendrites for the first time. This approach is adapted from the synthesis developed in the Chapter 2 by introducing a secondary ion in the reaction. Because the electrochemical reduction of Cu/Cu^{2+} pair is less than that of Pt/Pt(IV), the Pt precursor is reduced first. As a result, the final shape of the Pt-Cu alloys is governed by that of the Pt seeds, forming dendritic nanostructures. We further evaluate the catalytic activity of these nanostructures for electrooxidation of methanol and compare with commercially-available Pt/C catalysts.

3.2. Experimental

3.2.1 Materials. Dihydrogen hexachloroplatinate hexahydrate ($H_2PtCl_6 \bullet (H_2O)_6$, Alfa),

polyvinylpyrrolidone (PVP 55K, M.W. = 55,000, Aldrich), hydrochloric acid (HCl, 99.9999% metal basis, Alfa), copper(II) chloride ($CuCl_2$, Alfa), copper(II) sulfate ($CuSO_4$, Alfa), copper(II) acetate ($Cu(CH_3COO)_2$, Alfa), copper(II) nitrate ($Cu(NO_3)_2$, ethylene glycol (EG, J.T. Baker), polyethylene glycol (PEG, M.W. = 200, J.T. Baker), ferric chloride ($FeCl_3$, Spectrum), nitric acid (HNO_3, 99.9999% metal basis, Alfa), sodium chloride (NaCl, Alfa), citric acid ($C_6H_8O_7$, Alfa), sodium borohydride ($NaBH_4$, Alfa), polyvinylpyrrolidone (PVP 40K, M.W. = 40K, Alfa), polyvinylpyrrolidone (PVP 8K, M.W. = 8,000 Alfa), ascorbic acid (AA, EM Science), acetic acid (HAc, 99.7%, Alfa), perchloric acid ($HClO_4$, 99.9985% metal basis, Alfa), ethanol (EtOH, Koptec), and acetone ($(CH_3)_2CO$, EMD Chemicals) were used without further purification.

3.2.2. Synthesis of Pt-Cu Nanostructures. This method is a two-step procedure modified from the previous polyol synthesis reported by Chen, J. *et.al.*[9,10] and the synthesis from Chapter 2. For a typical synthesis, 4 mL of EG was heated at 110 °C for 1 h in a 25 mL three-neck round-bottom flask equipped with a condenser in atmosphere. Five solutions were prepared in separate vials: 2 mL of H_2PtCl_6 (0.033g, 31.08 mmol) in EG, 2 mL of Cu(II) precursor (varied concentrations), 2 mL of PVP 55K (0.045g, 0.409 mmol), HCl (50 mM), and $FeCl_3$ (200 mM) in EG. After 1 h, 100 μL of $FeCl_3$ and 50 μL of HCl was added to the reaction, following by injecting H_2PtCl_6, Cu(II) precursor, and PVP solutions simultaneously. The reaction was allowed heating for 24 h at 110 °C before the addition of a stronger reducing agent. The reaction mixture turned from orange yellow to green yellow, indicating the presence of Pt(II) and Cu(II). In the second step, AA (500 mM) in 0.5 mL EG was injected the reaction mixture. The reaction solution turned from yellow green to dark brown in 10 min, indicating the formation of Pt nanoparticles. The reaction was continued for another 30 min at 110 °C. The product was purified from the reactants and solvent by adding acetone with volume ratio > 5 and the centrifugation, following by washing with ethanol twice. The final pellet was suspended in 18 Ω

water for further use.

3.2.3. Instrumentation. TEM images were taken on a JEOL 100 CX electron microscope using a 100 kV accelerating voltage. The sample was prepared by dropping 5 μL of nanoparticle aqueous suspension on a formvar-coated copper grid. The grid was dried in air either held by a self-closed tweezers or on filter paper. X-ray diffraction (XRD) patterns were acquired using a Rigaku MiniFlex X-ray diffractometer equipped with Cu Kα radiation source operated at 30 kV/15 mA. The concentrations of Pt and other metals were determined using a GBC 932 atomic absorption spectrometer (AAS). An aliquot (200 μL) of nanoparticle suspension was digested with aqua regia (3:1 v/v ratio of HCl and HNO_3) before dilution in the matrix for the AAS measurement. The calibration curve was used to determine the concentration of Pt nanoparticle sample. UV-vis spectra were taken on an HP 8453 UV-visible spectrophotometer.

3.2.4. Electrocatalytic Activity of Pt Nanostructures. The electrocatalytic activity of the Pt-Cu nanodendrites and commercial Pt/C (20 wt%) catalysts were characterized by cyclic voltammetry (CV) and chronoamperometry (CA) on a CHI760 electrochemical workstation at room temperature. The measurements were performed using a three-electrode cell with the Ag/AgCl/1.0 M KCl electrode (E^o = -0.294 V vs. RHE) and Pt wire as reference and counter electrode, respectively. Glassy carbon disk (0.070 cm^2) was polished to a mirror finish before each experiment and was used as substrate for the working electrode. The catalyst suspension was prepared by mixing 1:1 volume of 0.4 mg_{Pt}/mL nanoparticle suspension with 0.05 wt% Nafion, followed by sonicating for 5 min. A 5 μL aliquot of the suspension was pipetted onto the glassy carbon substrate, yielding a Pt loading of 2 μg or 28 μg/cm^2. The working electrode was dried at room temperature. The electrochemical active surface area (ECSA) was determined from CV profile obtained at a scan rate of 50 mV/s in 0.1 M $HClO_4$ solution. The methanol oxidation was carried out in a solution containing 1.0 M CH_3OH and 0.1 M $HClO_4$ at a scan rate of 50

mV/s. The CA was recorded at 0.9 V vs. RHE in a solution containing 1.0 M CH_3OH and 0.1 M $HClO_4$. The electrochemical dealloying process was carried out at a scan rate of 50 mV/s with the potential range from 0 to 1.2 V vs. RHE in 0.1 M $HClO_4$ solution. After a certain number of cycles, the CV profile was recorded at a scan rate of 50 mV/s.

3.3. Result and Discussion

3.1.1. Synthesis

Figure 3-1, illustrates a co-reduction method of Pt and Cu by adding Cu precursors in the procedure described previously in Chapter 2. In this co-reduction approach Pt(IV) has a higher reduction potential as compared to Cu(II), thereby being reduced in the first step to Pt(0) and is etched and separated as seeds for the fast co-reduction of Pt-Cu in the second step to form Pt-Cu dendrite and nanostructures.[10, 11] Four different Cu(II) precursors were used including, $Cu(NO_3)_2$,

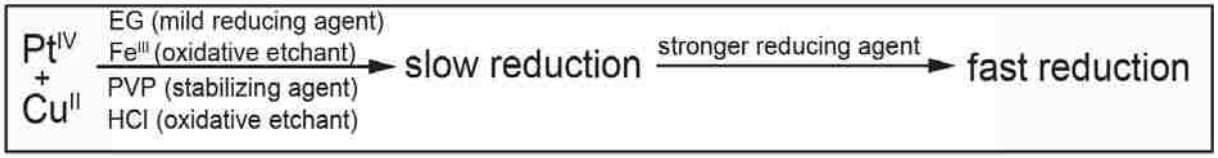

Figure 3-1. Schematic illustration of the overall strategy for the synthesis of Pt-Cu alloyed structure via seeded co-reduction.

$Cu(CH_3COO)_2$, $CuSO_4$, and $CuCl_2$, at 1:1 mole ratio of Pt(IV) to Cu(IV). The presence of different anions play a role in the final morphology of the nanostructures. For example, nitrate can act as an oxidizing agent.[11] As a result, the seed formation in the first step was obstructed, because no template to guide the growth in the second step for the thermodynamically favored spherical particles were formed (Fig. 3-2A).[12] The $Cu(CH_3COO)_2$ precursor yielded clusters of nanoparticles (Fig. 3-2B) while $CuSO_4$ and $CuCl_2$ gave individual small branched nanostructures. This is possibly due to the counter ions originating form a weak acid or strong acid.

We then further studied the effect of the precursor ratio on the final composition of the

nanostructures. For $CuSO_4$ precursors, the morphology of the Pt-Cu nanostructures remained to be small branched structures or dendrites with a size of 10-20 nm (Fig. 3-3). For $CuCl_2$, Figure 3-4 A-D, shows the TEM images of the products by varying the Pt-Cu precursor ratio from 3:1 to 1:7. The nanostructure of samples in (A) and (B) were found to be small agglomerates of branched nanoparticles with overall size of ~30 nm. In comparison the nanostructures in samples (C) and (D) were individual ultra-small branched nanoparticles with size of 10 nm. Their XRD patterns were plotted in Figure 3-4 E-H.

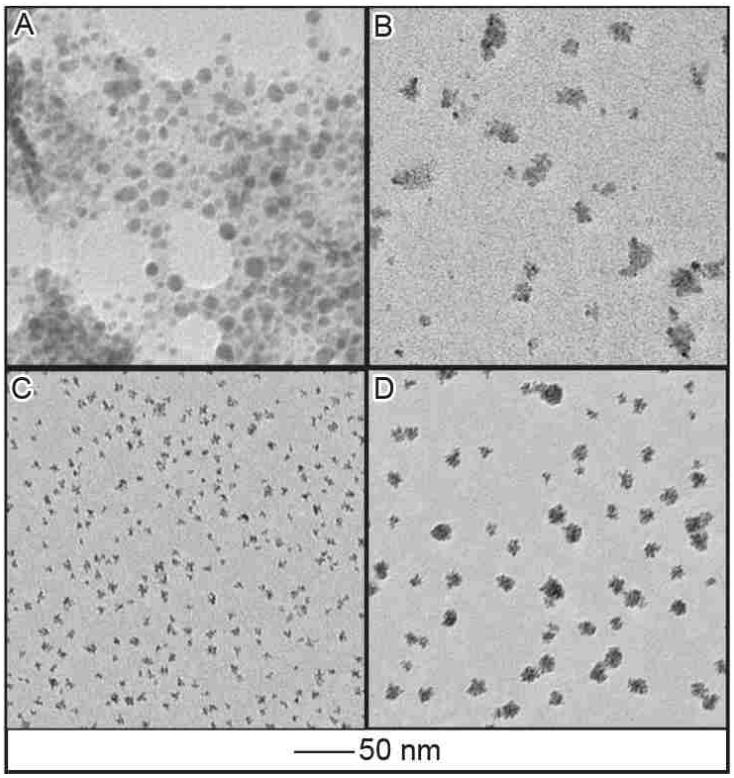

Figure 3-2. TEM images of Pt-Cu alloyed nanostructures synthesized by the co-reduction method using different Cu precursors. (**A)** *$Cu(NO_3)_2$,* **(B)** *$Cu(CH_3COO)_2$,* **(C)***$CuSO_4$,* **(D)***$CuCl_2$.*

The composition of the Pt-Cu alloys in the final nanostructures was calculated from the XRD data obtained. The relative percentages of Cu and Pt can be calculated using Bragg's Law:

$$2dsin\theta = n\lambda \qquad (1)$$

Where n is an integer that indicates which atomic layer diffraction acquired; this value is equal to one. The value of λ is the wavelength of incident x-ray light on the sample, 0.154 nm. Theta, θ, is the angle between the incident x-ray and the scattering plane which for all calculations is the [111] plane because it produced the most intense signal for all XRD patterns. Finally, d represents the spacing between the planes in the atomic lattice and in this equation:

$$d = \frac{a}{\sqrt{h^2+k^2+l^2}} \qquad (2)$$

In this equation a is the lattice spacing of the cubic crystal for each element and the values can be looked up based off of well documented experiments.[13] Terms h, k, and l are the Miller indices

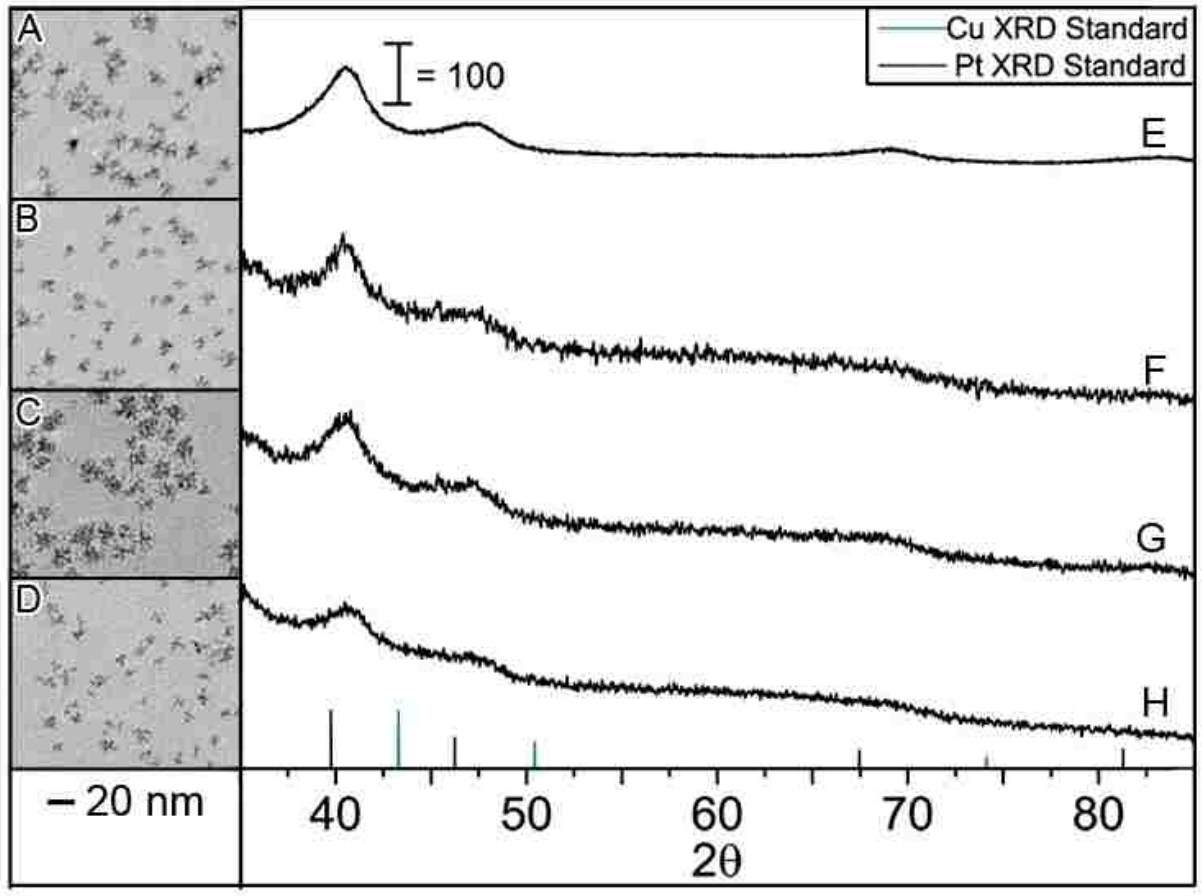

Figure 3-3. TEM images of Pt-Cu alloyed nanostructures synthesized by the seeded co-reduction method at different precursor ratios of H_2PtCl_6 *:* $CuSO_4$*.* **(A)** *2-1,* **(B)** *3-2,* **(C)** *1-1,* **(D)** *1-2.* **E-H** *the corresponding XRD patterns for the samples in* **A-D***, respectively.*

of the Braggs plane. Equation 1 and 2 can be combined to come up with the relation in Equation 3:

$$\left(\frac{\lambda}{2a}\right)^2 = \frac{\sin^2\theta}{h^2+k^2+l^2} \qquad (3)$$

Using the relationship in Equation 3 the lattice spacing, a, can be calculated for each alloy sample. The percentage of the Pt and Cu in the alloys can be calculated using the crystal spacing for Pt and Cu. The equation relating a bimetallic alloy is Vegard's Law[14]:

$$a_{alloy} = xa_{Pt} + (1-x)a_{Cu} \qquad (4)$$

In Equation 4, χ represents the mole fraction of Pt in the alloy sample. The values of α_{Pt} = 3.912 Å and α_{Cu} = 3.601 Å. The value of α_{alloy} is measured from the XRD patters. The mole fraction for Cu was calculated assuming:

$$1 - \chi_{(Pt)} = \chi_{(Cu)} \qquad (5)$$

The results of each synthesis were summarized in Table 3-1. The composition in either case, $CuSO_4$ or $CuCl_2$ appeared to be random. The precursor ratio has little effect on the final

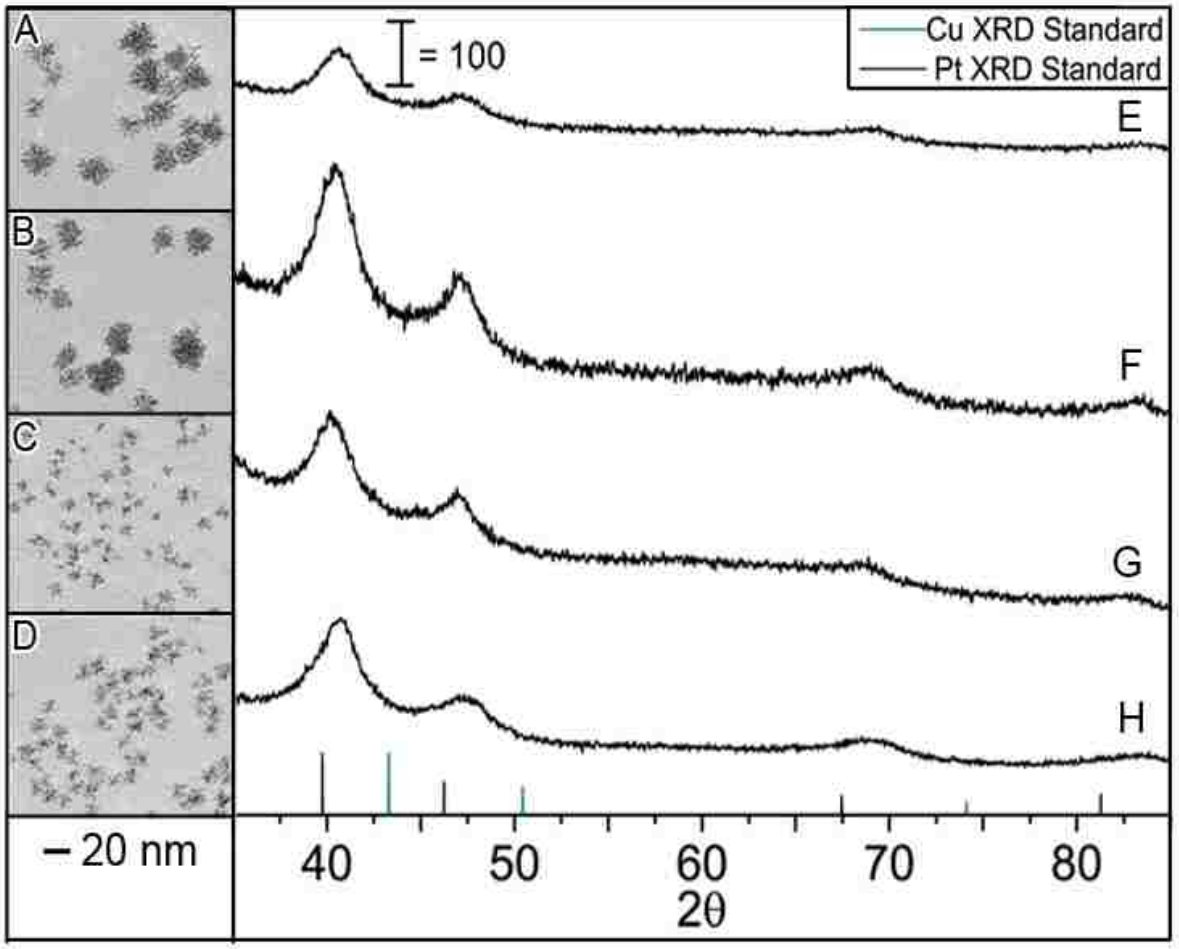

Figure 3-4. TEM images of Pt-Cu alloyed nanostructures synthesized by the co-reduction method at different precursor ratios of H_2PtCl_6 : $CuCl_2$. **(A)** *3-1,* **(B)** *1-1,* **(C)** *1-3,* **(D)** *1-7.* **E-H** *the corresponding XRD patterns for the samples in* **A-D**, *respectively.*

composition of Pt-Cu in the alloy at this temperature. To further verify the composition of the alloy the atomic absorption spectroscopy (AAS) was performed on each sample. The results for the $CuCl_2$ synthesis samples are listed in Table 3-2. This discrepancy between the AAS and XRD

data might be due to the adsorption of unreacted Pt at Cu ions on the surface of nanoparticles. For this reason the XRD pattern is more accurate to elucidate the composition of the alloy.

Increasing the temperature may facilitate the alloying process during the synthesis.[13, 15]

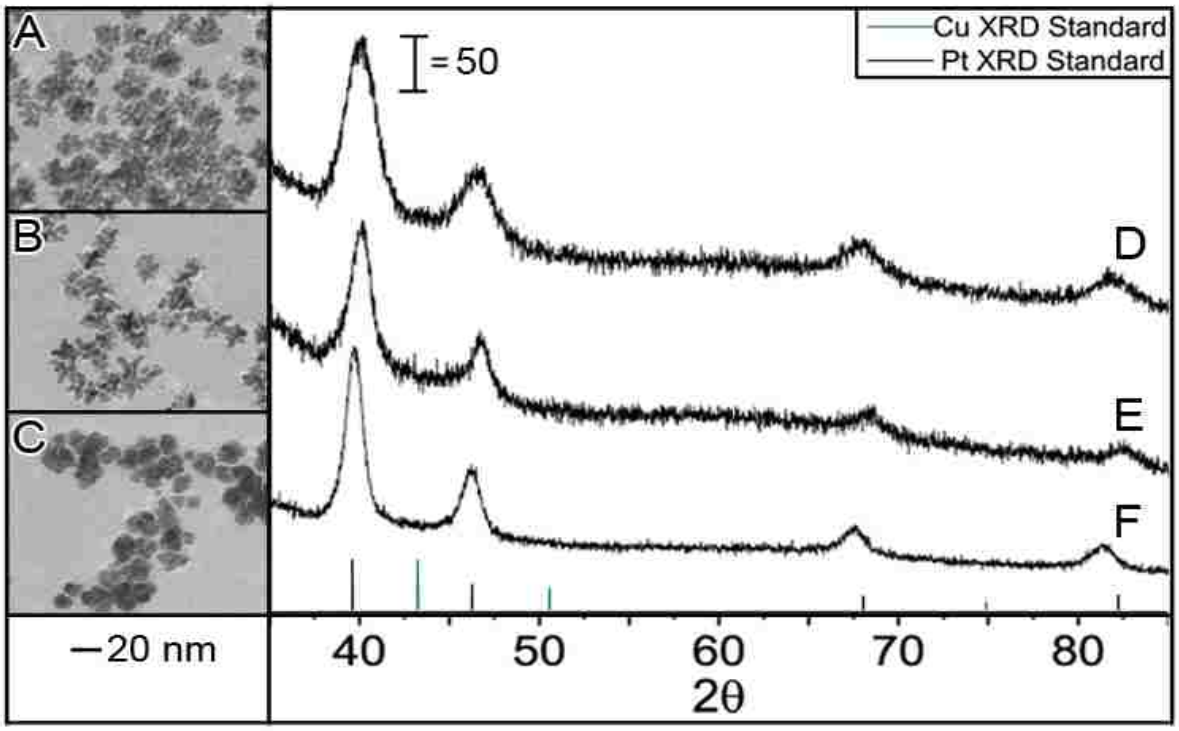

Figure 3-5. TEM images of Pt-Cu alloy particles using different nucleation heating temperatures. **(A)** *150°C,* **(B)** *185°C,* **(C)** *210°C.Graphs* **D-F** *are the corresponding XRD spectra for images* **A-C**, *respectively.*

To perform the synthesis at a higher temperature the solvent was changed from EG (b.p. 197.3 °C) to DEG (b.p. 244 °C). Figure 3-5, A-C, shows TEM images of the products from the reactions at 150 °C, 185 °C, and 210 °C, respectively. Due to the change of solvent and temperature slightly larger dendrites were formed. As temperature increased the branched nanoparticles became spherical at 210 °C. The XRD patterns, Fig. 3-5, D-F, indicated that the composition of the corresponding samples were $Pt_{63}Cu_{37}$, $Pt_{56}Cu_{44}$, and $Pt_{80}Cu_{20}$ for A, B, and C, respectively. This result suggested that the Pt precursor was reduced faster than the Cu precursor at higher temperatures. Further investigation needs to be conducted by extending the reaction time for the fast reduction step at 150 °C and 180 °C, respectively.

3.3.2. Electrochemical Measurements

Precursor Ratio (H_2PtCl_6 : $CuSO_4$)	XRD Pt%	XRD Cu%
2:1	56	44
3:2	53	47
1:1	64	36
1:2	61	39
Precursor Ratio (H_2PtCl_6 : $CuSO_4$)	XRD Pt%	XRD Cu%
3:1	57	43
1:1	64	36
1:3	68	32
1:7	48	52

Table 3-1. The list of corresponding composition information of the samples in Figure 3-3 and 3-4. The data was determined from the XRD analysis.

The samples in Fig. 3-4, A-C, were further evaluated for their electrochemical activity on MOR. The Pt concentration of each samples was measured by AAS. As prepared the surface of nanoparticle was covered by PVP which is soluble in water and had to be removed. Generally, PVP has little effect on the electrocatalytic activity of nanoparticle. [16] From the previous study in chapter 2, too much PVP may compromise the electrical conductivity. For each sample they were diluted to a final concentration of 0.4 mg_{Pt}/mL with nafion as was done in Chapter 2. Half of each sample was treated with 50% acetic acid (5:1 v/v nanostructures: HAc), then heated for 3 h at 60 °C for comparison. Figure 3-6 shows electrochemical measurements for three samples without the acetic acid treatment, while Figure 3-7 shows the electrochemical measurements for the three samples treated with acetic acid. From Figure 3-6 the ECSA for each sample is calculated to be $Pt_{57}Cu_{43}$ = 5.37 cm^2g^{-1}, $Pt_{64}Cu_{36}$ = 2757.81 cm^2g^{-1}, $Pt_{68}Cu_{32}$ = 480.95 cm^2g^{-1}, and Pt/C = 1173.62 cm^2g^{-1}. After acetic acid treatment the ECSA appeared to increase for $Pt_{57}Cu_{43}$ = 106.17 cm^2g^{-1} and $Pt_{64}Cu_{36}$ = 4568.86 cm^2g^{-1} but decreased for $Pt_{68}Cu_{32}$ = 369.70 cm^2g^{-1}. In both cases the ECSA of the $Pt_{64}Cu_{36}$ appeared to be the highest. This is possibly due to the morphology differences of the

Precursor Ratio (H_2PtCl_6 : $CuCl_2$)	Cu (mg/mL)	Pt (mg/mL)
3:1	0.097	0.144
1:1	0.039	0.109
1:3	0.099	0.204
1:7	0.045	0.204

Table 3-2. The list of composition information of the corresponding samples in Figure 3-4. The data was determined form AA measurements.

nanostructures.[17] Table 3-3 shows the results for the peak current densities of the forward (J_f) sweep and the ratios of the J_f to J_b (backward sweep) peaks. The CV profiles for each sample were obtained at two different scan rates, 10 mV/s and 50 mV/s. Generally, the slower the scan

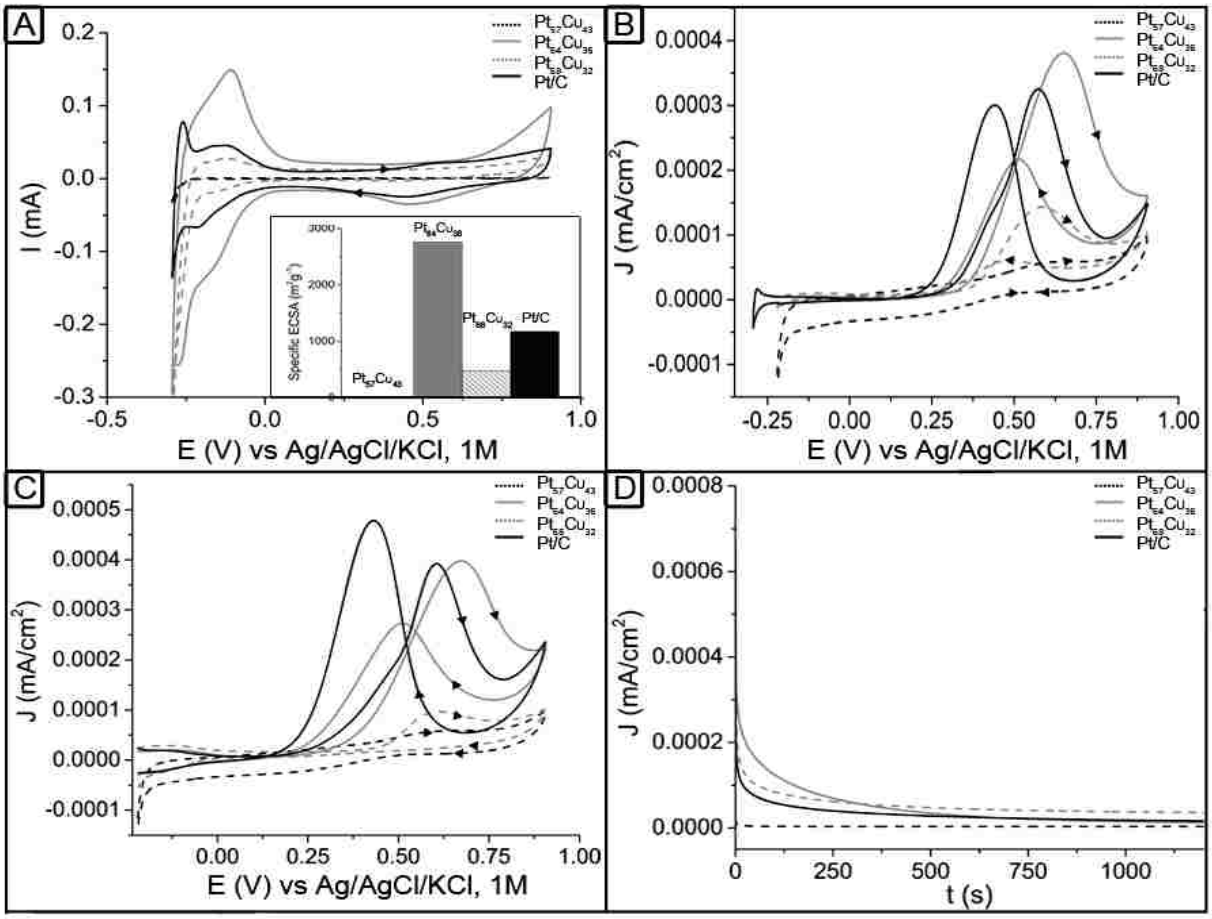

Figure 3-6. Electrochemical measurements of Pt-Cu alloyed nanostructures before acetic acid treatment. **(A)** *Cyclic voltammetric (CV) profiles in a 0.1 M $HClO_4$ solution at 50 mV/s, inset is the plot of the specific electrochemical surface area for the specific alloy ratios from left to right, 5.37, 2757.81, 480.95, and 1173.62 cm^2.* **(B-C)** *Cyclic voltammetric and* **(D)** *Chronoamperometry (CA) results of MeOH oxidation in a 0.1 M $HClO_4$ and 1 MeOH solution at* **(B)** *10 mV/s and* **(C)** *50 mV/s. CA curves were recorded at 1V vs. Ag/AgCl/KCl, 1M.*

rate is the easier the adsorbed species is stripped off. As a result, the J_f/J_b decreases as the scan rate increases. The discrepancy is possibly due to the stability of the catalysts. In all cases, the J_f/J_b increases in the order of $Pt_{57}Cu_{43} > Pt_{68}Cu_{32} > Pt_{64}Cu_{36} > Pt/C$. It is implied that the presence of Cu in the alloy improved the catalytic activity for MOR. The surface treatment and the

morphology also play a role in the electrocatalytic activity of the catalyst which will need to be further analyzed.

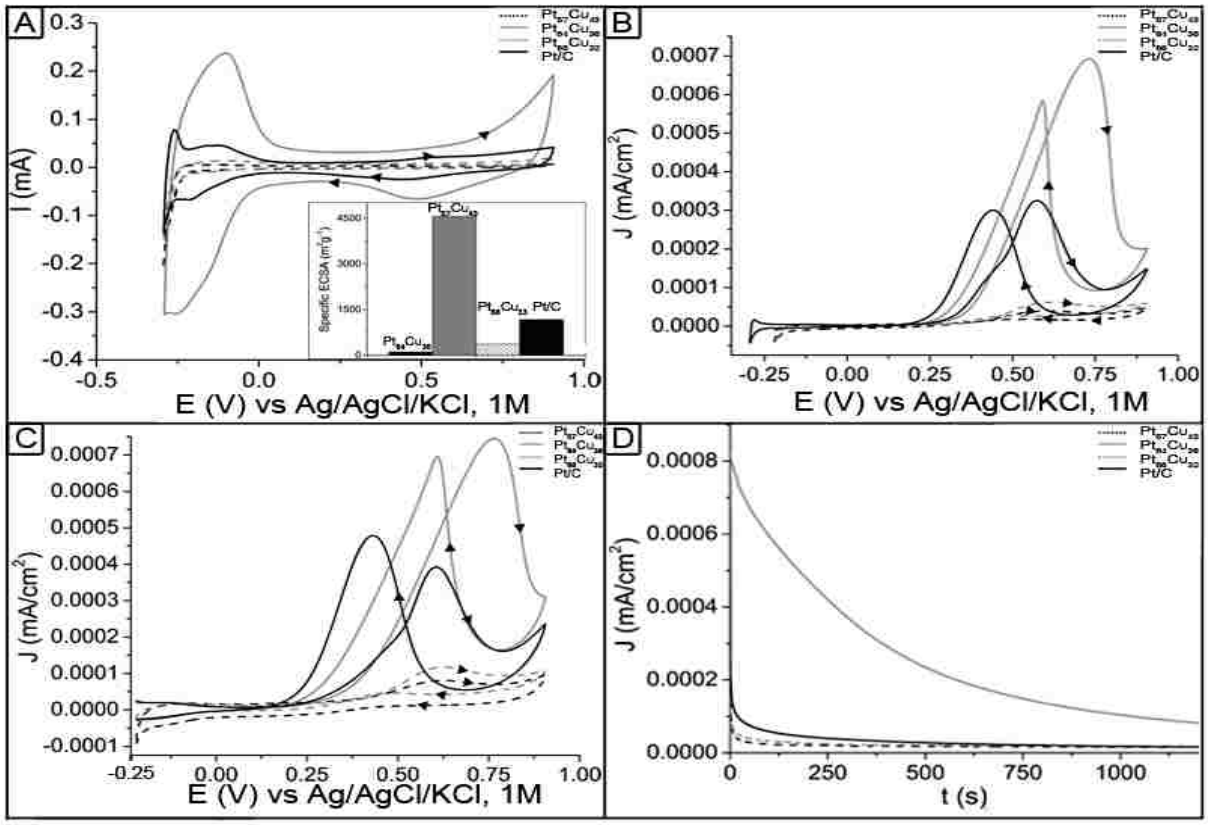

Figure 3-7. Electrochemical measurements of Pt-Cu alloyed nanostructures after acetic acid treatment. **(A)** *Cyclic voltammetric (CV) profiles in a 0.1 M $HClO_4$ solution at 50 mV/s, inset is the plot of the specific electrochemical surface area for the specific alloy ratios from left to right, 106.17, 4568.86, 369.70, and 1173.62 cm^2.* **(B-C)** *Cyclic voltammetric and* **(D)** *Chronoamperometry (CA) results of MeOH oxidation in a 0.1 M $HClO_4$ and 1 MeOH solution at* **(B)** *10 mV/s and* **(C)** *50 mV/s. CA curves were recorded at 1V vs. Ag/AgCl/KCl, 1M.*

3.4. Conclusion

In summary, Pt-Cu nanodendrites have been synthesized by a two-step co-reduction method involving a kinetically-controlled slow reduction and a subsequent fast reduction. The dendritic nanostructures were the result of the overgrowth on the {111} facets and the coalescence of the small dendritic seeds. The size and composition of the Pt-Cu nanodendrites were increased by

lengthening reaction time during the slow reduction. This method provides a facile synthesis for Pt-containing alloyed nanodendrites. The Pt_3Cu nanodendrites exhibit superior electrocatalytic activity for methanol oxidation as compared to Pt_3Cu nanoparticles and Pt/C catalyst.

3.5. References

1. Rossmeisl, J., Mavrikakis, M. et. al., Bifunctional anode catalysts for direct methanol fuel cells. *Energy Enviro. Sci.* **2012,** *5*, 8335-8342.

2. Yin, A. X., Min, X. Q., Zhu, W., Liu, W. C., Zhang, Y. W., Yan, C. H., Pt-Cu and Pt-Pd-Cu Concave Nanocubes with High-Index Facets and Superior Electrocatalytic Activity. *Chemistry – A European Journal* **2012,** *18*, 777-782.

3. Chen, J. e. a., Mesoporous hollow PtCu nanoparticles for electrocatalytic oxygen reduction reaction. *J. Mater. Chem. A* **2013,** *1*, 2391-2394.

4. Xia, B. Y., Wu, H. B., Wang, X., Lou, X. W., One-Pot Synthesis of Cubic $PtCu_3$ Nanocages with Enhanced Electrocatalytic Activity for the Methanol Oxidation Reaction. *J. Am. Chem. Soc.* **2012,** *134*, 13934-13937.

5. Liu, Q., Yan, Z., Henderson, N. L., Bauer, J. C., Goodman, D. W., Batteas, J. D., Schaak, R. E., Synthesis of CuPt Nanorod Catalysts with Tunable Lengths. *J. Am. Chem. Soc.* **2009,** *131*, 5720-5721.

6. Zhou, S., Varughese, B., Eichhorn, B., Jackson, G., McIlwrath, K., Pt–Cu Core–Shell and Alloy Nanoparticles for Heterogeneous NOx Reduction: Anomalous Stability and Reactivity of a Core–Shell Nanostructure. *Angewandte Chemie International Edition* **2005,** *44*, 4539-4543.

7. Lim, B., Jiang, M., Camargo, P. H. C., Cho, E. C., Tao, J., Lu, X., Zhu, Y., Xia, Y., Pd-Pt Bimetallic Nanodendrites with High Activity for Oxygen Reduction. *Science* **2009,** *324*, 1302-1305.

8. Chen, W.; Yu, R.; Li, L.; Wang, A.; Peng, Q.; Li, Y., A Seed-Based Diffusion Route to Monodisperse Intermetallic CuAu Nanocrystals. Angew. Chem. Int. Ed. **2010**, 49, 2917-2921.

9. Chen, J., Herricks, T., Xia, Y., Polyol Synthesis of Platinum Nanostructures: Control of Morphology through the Manipulation of Reduction Kinetics. *Angew. Chem. Int. Ed.* **2005,** *44*, 2589-2592.

10. Chen, J., Herricks, T., Xia, Y., Single-Crystal Nanowires of Platinum Can Be Synthesized by Controlling the Reaction Rate of a Polyol Process. *J. Am. Chem. Soc.* **2004,** *126*, 10854-10855.

11. Chen, S., Jenkins, S., Tao, J., Zhu, Y., Chen, J., Anisotropic Seeded Growth of Cu-M (M=Au, Pt, or Pd) Bimetallic Nanorods with Tunable Optical and Catalytic Properties. *J. Phys. Chem. C* **2013**.

12. Epron, F., Gauthard, F., Pinéda, C., Barbier, J., Catalytic Reduction of Nitrate and Nitrite on Pt–Cu/Al_2O_3 Catalysts in Aqueous Solution: Role of the Interaction between Copper and Platinum in the Reaction. *J. Cataly.* **2001,** *198*, 309-318.

13. Bond, W., Precision lattice constant determination. *Acta Crystal.* **1960,** *13*, 814-818.

14. Denton, A. R., Ashcroft, N. W., Vegard's law. *Phys. Rev. A* **1991,** *43*, 3161-3164.

15. Garcia-Gutierrez, D. I., Gutierrez-Wing, C. E., Giovanetti, L., Ramallo-López, J. M., Requejo, F. G., Jose-Yacaman, M., Temperature Effect on the Synthesis of Au−Pt Bimetallic Nanoparticles. *J. Phys. Chem. B* **2005,** *109*, 3813-3821.

16. Chen, J., Lim, B., Lee, E. P., Xia, Y., Shape-controlled synthesis of platinum nanocrystals for catalytic and electrocatalytic applications. *Nano Today* **2009,** *4*, 81-95.

17. Wolf V., H. A. G., Arnold L., *Handbook of Fuel Cells - Fundamentals, Technology and Applications*. John Wiley & Sons, Ltd.: **2003**; Vol. 2.

Chapter 4: Conclusions

Using a two-step procedure synthesis was developed to successfully generate both branched Pt nanostructures and dendritic Pt-Cu nanostructures in a reasonably-high yield. It was determined that the presence of oxidative etchants such as Fe(III), Cl^-, and O_2, are essential to obtain the single-crystalline seeds with {111} facets activated for overgrowth. In the second step, a stronger reducing agent, AA, was used to introduce a fast reduction process to shorten the reaction time and produce the branched nanostructure in high yield. The large aggregate in the products for each synthesis can be purified easily using centrifugation techniques.

The Pt branched nanostructures and Pt-Cu were studied for their electrochemical activity as a catalyst for MOR. As compared to the commercially-available Pt/C, the Pt branched nanostructures have a lower normalized $ECSA/g_{Pt}$ possibly due to the lack of carbon support and the presence of agglomeration of the Pt nanostructures. The Pt branched nanostructures exhibit less poisoning by CO_{ad} species from MOR possibly due to the presence of more active sites as compared to the Pt nanoparticles. Further analysis of the nanostructures is needed. Of the Pt-Cu nanostructures the Pt_3Cu nanodendrites exhibit superior electrocatalytic activity for methanol oxidation as compared to Pt_3Cu nanoparticles and Pt/C catalyst. These Pt and Pt-Cu nanostructures have future applications for development of efficient methanol fuel cells. The synthesis needs further investigation to optimize the ECSA and current densities of both products to produce the best product for fuel cell applications. Also Pt-M alloys involving other metals that also exhibit improved resistance to poisoning effects and greater ECSA can be investigated.

Greater characterization by EDX mapping, XPS, and HR-TEM can be examined to better understand the final product and possible methods for improving the growth mechanism.